View metadata, citation and similar papers at core.ac.uk

brought to you by CORE

provided by University of Bath Research Portal

Citation for published version:
Blackburn, OA, Coe, BJ, Helliwell, M, Ta, YT, Peter, LM, Wang, H, Anta, JA & Guillén, E 2013, 'Ruthenium(II) dichloro or dithiocyanato complexes with 4,4:2,2:4,4-quaterpyridinium ligands: Towards photosensitisers with enhanced low-energy absorption properties', Polyhedron, vol. 50, no. 1, pp. 622-635. https://doi.org/10.1016/j.poly.2012.09.049

DOI:
10.1016/j.poly.2012.09.049

Publication date:
2013

Document Version
Peer reviewed version

Link to publication

NOTICE: this is the author's version of a work that was accepted for publication in Polyhedron. Changes resulting from the publishing process, such as peer review, editing, corrections, structural formatting, and other quality control mechanisms may not be reflected in this document. Changes may have been made to this work since it was submitted for publication. A definitive version was subsequently published in Polyhedron, vol 50, issue 1, 2013, DOI 10.1016/j.poly.2012.09.049

University of Bath

General rights
Copyright and moral rights for the publications made accessible in the public portal are retained by the authors and/or other copyright owners and it is a condition of accessing publications that users recognise and abide by the legal requirements associated with these rights.

Take down policy
If you believe that this document breaches copyright please contact us providing details, and we will remove access to the work immediately and investigate your claim.

Download date: 13. May. 2019

*Manuscript
Click here to view linked References

Ruthenium(II) dichloro or dithiocyanato complexes with 4,4′:2′,2″:4″,4‴-quaterpyridinium ligands: towards photosensitizers with enhanced low-energy absorption properties

Octavia A. Blackburn,[a] Benjamin J. Coe*,[a] Madeleine Helliwell,[a] Yien T. Ta,[a] Laurence M. Peter[b], Hongxia Wang,[b] Juan A. Anta,[c] Elena Guillén[c]

[a] *School of Chemistry, University of Manchester, Oxford Road, Manchester M13 9PL, UK*

[b] *Department of Chemistry, University of Bath, Bath BA2 5NB, UK*

[c] *Area de Quimica Fisica, Departamento de Sistemas Físicos, Químicos y Naturales, Universidad Pablo de Olavide, 41013 Sevilla, Spain*

* Corresponding author. E-mail: b.coe@manchester.ac.uk; Fax +44 (0)161 275 4598; Tel +44 (0)161 275 4601.

ABSTRACT

Fourteen new complexes of the form *cis*-$[Ru^{II}X_2(R_2qpy^{2+})_2]^{4+}$ (R_2qpy^{2+} = a 4,4′:2′,2″:4″,4‴-quaterpyridinium ligand, X = Cl^- or NCS^-) have been prepared and isolated as their PF_6^- salts. Characterisation involved various techniques including ^1H NMR spectroscopy and +electrospray or MALDI mass spectrometry. The UV–vis spectra display intense intraligand $\pi \rightarrow \pi^*$ absorptions, and also metal-to-ligand charge-transfer (MLCT) bands with two resolved maxima in the visible region. Red-shifts in the MLCT bands occur as the electron-withdrawing strength of the pyridinium groups increases, while replacing Cl^- with NCS^- causes blue-shifts. Cyclic voltammograms show quasi-reversible or reversible $Ru^{III/II}$ oxidation waves, and several ligand-based reductions that are irreversible. The variations in the redox potentials correlate with changes in the MLCT energies. A single-crystal X-ray structure has been obtained for a protonated form of a proligand salt, $[(4\text{-}(CO_2H)Ph)_2qpyH^{3+}][HSO_4]_3 \bullet 3H_2O$. Time-dependent density functional theory calculations give adequate correlations with the experimental UV–vis spectra for the two carboxylic acid-functionalised complexes in DMSO. Despite their attractive electronic absorption spectra, these dyes are relatively inefficient photosensitizers on electrodes coated with TiO_2 or ZnO. These observations are attributed primarily to weak electronic coupling with the surfaces, since the DFT-derived LUMOs include no electron density near the carboxylic acid anchors.

1. Introduction

The urgent requirement to develop sources of clean and renewable energy has stimulated much interest in dye-sensitized solar cells (DSSCs) [1]. The general field of solar energy conversion is broad and includes many competing but related technologies [1g]. Commonly used silicon solar cells, which exploit photon absorption by a p-n semiconductor junction, require materials of high purity. More recently developed inorganic thin film materials, like cadmium telluride or copper indium gallium selenide, contain toxic or rare elements. In the light of such considerations, the 1991 report by O'Regan and Grätzel of efficient photosensitization of a wide band-gap semiconductor by a trinuclear ruthenium-based dye [2] inspired much subsequent research. Complexes of Ru and some other metals with polypyridyl ligands such as 2,2′-bipyridyl (2,2′-bpy) typically display intense absorptions in the visible region due to metal-to-ligand charge-transfer (MLCT) transitions.

A DSSC contains a nanoparticulate film of a semiconductor, most commonly TiO_2, coated with a dye monolayer. Most cells are based on a photoanode in which the photoexcited dye injects an electron into the conduction band of the semiconductor. The oxidised dye is then reduced back to its original state by a species in the electrolyte; this is usually an organic solvent containing the I^-/I_3^- couple, but solid 'hole transporting' materials are also attractive. To achieve high power conversion efficiences, a number of aspects must be considered, but synthetic chemists have naturally focused on the structure of the sensitizer molecule. Amongst the key criteria for potentially useful operation are strong absorption across the entire visible region and the near-UV/IR, appropriate energy matching with and strong electronic coupling to the electrode surface (typically via carboxylate anchors), and high stability over many photoredox cycles.

Ru complexes have featured extensively also in the field of nonlinear optical (NLO) compounds [3]. Previously, we have studied complexes of 4,4′:2′,2″:4″,4‴-quaterpyridinium ligands, R_2qpy^{2+} where R = Me, Ph, etc. These compounds include V-shaped dipoles with electron-donating *cis*-$\{Ru^{II}(NH_3)_4\}^{2+}$ centres [4], and octupolar tris-chelates with a $[Ru^{II}(2,2'\text{-bpy})_3]^{2+}$ core [5,6]. The MLCT absorption profiles of these complexes are especially broad

and intense, with the tris-chelates displaying two well-resolved bands. Pyridinium groups are often used in NLO chromophores [7], and as electron-accepting units in other photoactive molecular assemblies [8]. However, our recent report of *N*-arylstilbazolium species is the first time that pyridinium compounds have been used in DSSCs [9]. These purely organic dyes gave relatively modest efficiencies, but with substantial scope for improvement. In other work of some relevance, TiO_2-based photocathodes incorporating $[Ru^{II}(R_2qpy^{2+})_3]^{8+}$ chromophores (R = 2-carboxyethyl or 2-propylphosphonic acid) have been described [10]. We have investigated also complexes of the form *cis*-$[Ru^{II}(2,2'\text{-bpy})_2(R_2qpy^{2+})]^{4+}$; two carboxylic acid-functionalised derivatives were tested in DSSCs, but showed negligible activities, attributable at least in part to their $[Ru^{II}(2,2'\text{-bpy})_3]^{2+}$-based structures [11]. Here, we describe related complexes that contain the anionic thiocyanate coligand that is present in many of the most effective Ru-based sensitizers, together with analogous chloride species.

2. Experimental

2.1. Materials, procedures and physical measurements

All reactions were performed under an Ar atmosphere. The precursor complex *cis*-$Ru^{II}Cl_2(DMSO)_4$ [12] and the proligand salts *N*″,*N*‴-dimethyl-4,4′:2′,2″:4″,4‴-quaterpyridinium chloride, $[Me_2qpy^{2+}]Cl_2$ [11], *N*″,*N*‴-diphenyl-4,4′:2′,2″:4″,4‴-quaterpyridinium chloride, $[Ph_2qpy^{2+}]Cl_2$ [11], *N*″,*N*‴-di(4-acetylphenyl)-4,4′:2′,2″:4″,4‴-quaterpyridinium chloride, $[(4\text{-}AcPh)_2qpy^{2+}]Cl_2$ [11], *N*″,*N*‴-di(2-pyrimidyl)-4,4′:2′,2″:4″,4‴-quaterpyridinium chloride, $[(2\text{-}Pym)_2qpy^{2+}]Cl_2$ [11], *N*″,*N*‴-di(3,5-bismethoxycarbonylphenyl)-4,4′:2′,2″:4″,4‴-quaterpyridinium chloride, $[(3,5\text{-}MC_2Ph)_2qpy^{2+}]Cl_2$ [11] and *N*″,*N*‴-di(4-methoxycarbonylphenyl)-4,4′:2′,2″:4″,4‴-quaterpyridinium chloride, $[(4\text{-}MCPh)_2qpy^{2+}]Cl_2$ [11], were prepared according to published methods. All other reagents were obtained commercially and used as supplied. Products were dried overnight in a vacuum dessicator ($CaSO_4$) prior to characterisation.

^1H NMR spectra were recorded on a Bruker AV-400 or a Bruker AV-500 spectrometer and all shifts are referenced to TMS. The AA′BB′ patterns of pyridyl or phenyl rings are reported as simple doublets, with '*J* values' referring to the two most intense peaks. Elemental analyses were performed by the Microanalytical Laboratory, University of Manchester. IR spectroscopy was performed on solid samples by using an Excalibur BioRad FT-IR spectrometer, and UV–vis spectra were obtained by using a Shimadzu UV-2401 PC spectrophotometer. Mass spectra were measured by using MALDI on a Micromass Tof Spec 2e or +electrospray on a Micromass Platform II spectrometer with acetonitrile as the solvent. Cyclic voltammetric measurements were carried out with an Ivium CompactStat. An EG&G PAR K0264 single-compartment microcell was used with a silver/silver chloride reference electrode (3 M NaCl, saturated AgCl) separated by a salt bridge from a glassy carbon disk working electrode and Pt wire auxiliary electrode. Acetonitrile was freshly distilled (from CaH_2) and $[NBu^n_4]PF_6$, as supplied from Fluka, was used as the supporting electrolyte.

Solutions containing *ca*. 10^{-3} M analyte (0.1 M electrolyte) were deaerated by purging with N_2. All $E_{1/2}$ values were calculated from $(E_{pa} + E_{pc})/2$ at a scan rate of 200 mV s^{-1}.

2.2. Syntheses

2.2.1. N'',N'''-Di(3,5-biscarboxyphenyl)-4,4':2',2'':4'',4'''-quaterpyridinium chloride, [(3,5-$(CO_2H)_2Ph)_2qpy^{2+}]Cl_2$

$[(3,5\text{-}MC_2Ph)_2qpy^{2+}]Cl_2 \bullet 2H_2O$ (250 mg, 0.311 mmol) was added to *tert*-butanol (50 mL) followed by conc. H_2SO_4 (2 mL). The mixture was heated at reflux for 24 h. After cooling, a pale peach-coloured precipitate was filtered off, washed with copious amounts of water and dried. Yield: 227 mg (94%). δ_H (400 MHz, CD_3SOCD_3) 9.64 (4 H, d, J = 7.1 Hz, C_5H_4N), 9.12 (2 H, d, J = 5.3 Hz, C_5H_3N), 9.08 (2 H, d, J = 0.8 Hz, C_5H_3N), 8.94 (4 H, d, J = 7.1 Hz, C_5H_4N), 8.74 (2 H, t, J = 1.4 Hz, C_6H_3), 8.71 (4 H, d, J = 1.5 Hz, C_6H_3), 8.31 (2 H, dd, J = 5.2, 1.9 Hz, C_5H_3N). ν(C=O) 1699s cm^{-1}. Anal. Calcd (%) for $C_{36}H_{24}Cl_2N_4O_8 \bullet 3.5H_2O$: C, 55.8; H, 4.0; N, 7.2. Found: C, 56.1; H, 3.9; N, 7.1.

2.2.2. N'',N'''-Di(4-carboxyphenyl)-4,4':2',2'':4'',4'''-quaterpyridinium chloride, [(4-$(CO_2H)Ph)_2qpy^{2+}]Cl_2$

This compound was prepared in a manner similar to $[(3,5\text{-}(CO_2H)_2Ph)_2qpy^{2+}]Cl_2$ by using $[(4\text{-}MCPh)_2qpy^{2+}]Cl_2 \bullet 3.5H_2O$ (250 mg, 0.350 mmol) instead of $[(3,5\text{-}MC_2Ph)_2qpy^{2+}]Cl_2 \bullet 2H_2O$ to afford a cream-coloured solid. Yield: 187 mg (74%). δ_H (400 MHz, CD_3SOCD_3) 9.58 (4 H, d, J = 7.1 Hz, C_5H_4N), 9.11 (2 H, d, J = 5.3 Hz, C_5H_3N), 9.07 (2 H, dd, J = 1.8, 0.8 Hz, C_5H_3N), 8.94 (4 H, d, J = 7.1 Hz, C_5H_4N), 8.31– 8.27 (6 H, C_5H_3N + C_6H_4), 8.06 (4 H, d, J = 8.6 Hz, C_6H_4). ν(C=O) 1709s cm^{-1}. Anal. Calcd (%) for $C_{34}H_{24}Cl_2N_4O_4 \bullet 5.5H_2O$: C, 56.5; H, 4.9; N, 7.8. Found: C, 56.4; H, 4.5; N, 7.6.

*2.2.3. cis-[$Ru^{II}Cl_2(Me_2qpy^{2+})_2][PF_6]_4$ (**1**)*

cis-$Ru^{II}Cl_2(DMSO)_4$ (30 mg, 0.062 mmol) and $[Me_2qpy^{2+}]Cl_2 \bullet 3.1H_2O$ (51 mg, 0.109 mmol) were added to *n*-propanol (13 mL) and the mixture was heated under reflux for 7 h. A

solution of LiCl (53 mg, 1.25 mmol) in water (2 mL) was added, and the deep blue solution heated under reflux for 18 h. After cooling to room temperature, a dark blue precipitate was filtered off, washed with a little *n*-propanol and dried. This solid was dissolved in methanol (~20 mL). Addition of 1 M aqueous NH_4PF_6 afforded a dark blue precipitate which was filtered off, washed with water and dried. Yield: 48 mg (61%). δ_H (400 MHz, CD_3CN) 10.29 (2 H, d, J = 6.0 Hz, C_5H_3N), 9.09 (2 H, d, J = 1.3 Hz, C_5H_3N), 8.92 (2 H, d, J = 1.5 Hz, C_5H_3N), 8.86 (4 H, d, J = 6.8 Hz, C_5H_4N), 8.71 (4 H, d, J = 6.8 Hz, C_5H_4N), 8.65 (4 H, d, J = 6.8 Hz, C_5H_4N), 8.40 (4 H, d, J = 6.8 Hz, C_5H_4N), 8.19 (2 H, dd, J = 5.8, 1.8 Hz, C_5H_3N), 7.94 (2 H, d, J = 6.0 Hz, C_5H_3N), 7.45 (2 H, dd, J = 6.0, 1.5 Hz, C_5H_3N), 4.41 (6 H, s, Me), 4.31 (6 H, s, Me). Anal. Calcd (%) for $C_{44}H_{40}Cl_2F_{24}N_8P_4Ru{\bullet}H_2O$: C, 36.4; H, 2.9; N, 7.7. Found: C, 36.5; H, 2.5; N, 7.8. ES-MS: m/z = 1288 ($[M - PF_6]^+$), 571 ($[M - 2PF_6]^{2+}$).

All of the compounds **2**–**6** were prepared in a manner similar to **1**, by using the appropriate proligand salt to give dark blue solids.

*2.2.4. cis-[$Ru^{II}Cl_2(Ph_2qpy^{2+})_2$][$PF_6$]$_4$ (**2**)*

Used [Ph_2qpy^{2+}]$Cl_2{\bullet}H_2O$ (66 mg, 0.119 mmol). Yield: 64 mg (60%). δ_H (400 MHz, CD_3CN) 10.34 (2 H, d, J = 5.8 Hz, C_5H_3N), 9.26 (2 H, d, J = 2.0 Hz, C_5H_3N), 9.20 (4 H, d, J = 7.1 Hz, C_5H_4N), 9.10 (2 H, d, J = 1.8 Hz, C_5H_3N), 9.05 (4 H, d, J = 7.1 Hz, C_5H_4N), 8.88 (4 H, d, J = 6.8 Hz, C_5H_4N), 8.64 (4 H, d, J = 7.1 Hz, C_5H_4N), 8.26 (2 H, dd, J = 6.0, 1.5 Hz, C_5H_3N), 8.03 (2 H, d, J = 6.0 Hz, C_5H_3N), 7.90–7.81 (10 H, Ph), 7.77 (10 H, s, Ph), 7.58 (2 H, dd, J = 6.2, 1.6 Hz, C_5H_3N). Anal. Calcd (%) for $C_{64}H_{48}Cl_2F_{24}N_8P_4Ru{\bullet}5.5H_2O$: C, 43.2; H, 3.3; N, 6.3. Found: C, 43.1; H, 2.9; N, 6.3. MALDI-MS: m/z = 1537 ($[M - PF_6]^+$), 697 ($[M - 2PF_6]^{2+}$).

*2.2.5. cis-[$Ru^{II}Cl_2${(4-AcPh)$_2$qpy^{2+}}$_2$][PF_6]$_4$ (**3**)*

Used [(4-AcPh)$_2$qpy^{2+}]$Cl_2{\bullet}1.8H_2O$ (77 mg, 0.118 mmol). Yield: 76 mg (68%). δ_H (400 MHz, CD_3CN) 10.35 (2 H, d, J = 6.0 Hz, C_5H_3N), 9.24−9.22 (6 H, C_5H_4N + C_5H_3N), 9.09−9.06 (6 H, C_5H_4N + C_5H_3N), 8.87 (4 H, d, J = 6.8 Hz, C_5H_4N), 8.64 (4 H, d, J = 7.1 Hz,

C_5H_4N), 8.35 (4 H, d, J = 8.6 Hz, C_6H_4), 8.29−8.27 (6 H, C_5H_3N + C_6H_4), 8.05 (2 H, d, J = 6.0 Hz, C_5H_3N), 8.01 (4 H, d, J = 8.8 Hz, C_6H_4), 7.90 (4 H, d, J = 8.8 Hz, C_6H_4), 7.60 (2 H, dd, J = 6.3, 1.5 Hz, C_5H_3N), 2.72 (6 H, s, Me), 2.68 (6 H, s, Me). ν(C=O) 1681s cm^{-1}. Anal. Calcd for $C_{72}H_{56}Cl_2F_{24}N_8O_4P_4Ru•4H_2O$: C, 45.0; H, 3.4; N, 5.8. Found: C, 44.9; H, 2.9; N, 5.9. MALDI−MS: m/z = 1706 ($[M - PF_6]^+$).

*2.2.6. cis-[$Ru^{II}Cl_2${(2-Pym)$_2$qpy^{2+}}$_2$][PF_6]$_4$ (**4**)*

Used [(2-Pym)$_2$qpy^{2+}]Cl_2•2.3H_2O (67 mg, 0.115 mmol). Yield: 66 mg (65%). δ_H (400 MHz, CD_3CN) 10.41 (2 H, d, J = 6.3 Hz, C_5H_3N), 10.22 (4 H, d, J = 6.8 Hz, C_5H_4N), 10.05 (4 H, d, J = 7.3 Hz, C_5H_4N), 9.26 (2 H, s, C_5H_3N), 9.17 (4 H, d, J = 4.8 Hz, $C_4H_3N_2$), 9.10−9.08 (6 H, C_5H_3N + $C_4H_3N_2$), 8.91 (4 H, d, J = 6.8 Hz, C_5H_4N), 8.68 (4 H, d, J = 7.1 Hz, C_5H_4N), 8.33 (2 H, dd, J = 5.8, 1.5 Hz, C_5H_3N), 8.02 (2 H, d, J = 6.3 Hz, C_5H_3N), 7.91 (2 H, t, J = 4.9 Hz, $C_4H_3N_2$), 7.85 (2 H, t, J = 4.9 Hz, $C_4H_3N_2$), 7.58 (2 H, dd, J = 6.0, 1.5 Hz, C_5H_3N). Anal. Calcd (%) for $C_{56}H_{40}Cl_2F_{24}N_{16}P_4Ru•5H_2O$: C, 37.8; H, 2.8; N, 12.6. Found: C, 37.7; H, 2.3; N, 12.5. MALDI−MS: m/z = 1546 ($[M - PF_6]^+$).

*2.2.7. cis-[$Ru^{II}Cl_2${(3,5-MC_2Ph)$_2$qpy^{2+}}$_2$][PF_6]$_4$ (**5**)*

Used [(3,5-MC_2Ph)$_2$qpy^{2+}]Cl_2•2H_2O (95 mg, 0.118 mmol). Yield: 76 mg (58%). δ_H (400 MHz, CD_3CN) 10.37 (2 H, d, J = 6.0 Hz, C_5H_3N), 9.26−9.24 (6 H, C_5H_4N + C_5H_3N), 9.11 (4 H, d, J = 7.3 Hz, C_5H_4N), 9.08 (2 H, d, J = 1.8 Hz, C_5H_3N), 8.93 (4 H, d, J = 6.8 Hz, C_5H_4N), 8.89 (2 H, t, J = 1.4 Hz, C_6H_3), 8.84 (2 H, t, J = 1.4 Hz, C_6H_3), 8.69 (4 H, d, J = 1.5 Hz, C_6H_3), 8.67 (4 H, d, J = 7.1 Hz, C_5H_4N), 8.59 (4 H, d, J = 1.5 Hz, C_6H_3), 8.32 (2 H, dd, J = 6.0, 1.7 Hz, C_5H_3N), 8.04 (2 H, d, J = 6.3 Hz, C_5H_3N), 7.60 (2 H, dd, J = 5.7, 1.9 Hz, C_5H_3N), 4.02 (12 H, s, Me), 3.98 (12 H, s, Me). ν(C=O) 1721s cm^{-1}. Anal. Calcd (%) for $C_{80}H_{64}Cl_2F_{24}N_8O_{16}P_4Ru•5.5H_2O$: C, 42.8; H, 3.4; N, 5.0. Found: C, 42.3; H, 2.8; N, 5.2. MALDI−MS: m/z = 2002 ($[M - PF_6]^+$).

*2.2.8. cis-[$Ru^{II}Cl_2${(4-MCPh)$_2$qpy^{2+}}$_2$][PF_6]$_4$ (**6**)*

Used [(4-MCPh)$_2$qpy^{2+}]Cl_2•3.5H_2O (81 mg, 0.113 mmol). Yield: 79 mg (71%). δ_H (400 MHz, CD_3CN) 10.34 (2 H, d, *J* = 5.6 Hz, C_5H_3N), 9.23−9.21 (6 H, C_5H_4N + C_5H_3N), 9.07−9.05 (6 H, C_5H_4N + C_5H_3N), 8.88 (4 H, d, *J* = 6.1 Hz, C_5H_4N), 8.64 (4 H, d, *J* = 6.8 Hz, C_5H_4N), 8.39 (4 H, d, *J* = 8.6 Hz, C_6H_4), 8.33−8.27 (6 H, C_5H_3N + C_6H_4), 8.04 (2 H, d, *J* = 6.0 Hz, C_5H_3N), 8.00 (4 H, d, *J* = 8.6 Hz, C_6H_4), 7.88 (4 H, d, *J* = 8.8 Hz, C_6H_4), 7.59 (2 H, dd, *J* = 6.0, 1.8 Hz, C_5H_3N), 3.98 (6 H, s, Me), 3.95 (6 H, s, Me). δ_H (500 MHz, CD_3SOCD_3) 10.24 (2 H, d, *J* = 6.0 Hz, C_5H_3N), 9.77 (4 H, d, *J* = 6.6 Hz, C_5H_4N), 9.68 (2 H, s, C_5H_3N), 9.62 (4 H, d, *J* = 6.6 Hz, C_5H_4N), 9.51 (2 H, s, C_5H_3N), 9.17 (4 H, d, *J* = 6.6 Hz, C_5H_4N), 8.90 (4 H, d, *J* = 6.6 Hz, C_5H_4N), 8.77 (2 H, dd, *J* = 5.8, 1.4 Hz, C_5H_3N), 8.39 (4 H, d, *J* = 8.5 Hz, C_6H_4), 8.33 (4 H, d, *J* = 8.5 Hz, C_6H_4), 8.19 (4 H, d, *J* = 8.5 Hz, C_6H_4), 8.09 (4 H, d, *J* = 8.8 Hz, C_6H_4), 8.06 (2 H, d, *J* = 5.8 Hz, C_5H_3N), 7.93 (2 H, dd, *J* = 6.3, 1.6 Hz, C_5H_3N), 3.98 (6 H, s, Me), 3.94 (6 H, s, Me). ν(C=O) 1717s cm^{-1}. Anal. Calcd (%) for $C_{72}H_{56}Cl_2F_{24}N_8O_8P_4Ru$•3$H_2O$: C, 44.0; H, 3.2; N, 5.7. Found: C, 43.9; H, 2.7; N, 5.9. ES−MS: *m*/*z* = 1768 ([M − PF_6]$^+$).

*2.2.9. cis-[$Ru^{II}Cl_2${[4-(CO_2H)Ph]$_2$qpy^{2+}}$_2$][PF_6]$_4$ (**7**)*

[(4-(CO_2H)Ph)$_2$qpy]Cl_2•5.5H_2O (129 mg, 0.179 mmol) was added to 2-methoxyethanol (25 mL) and the mixture was heated to reflux in an oil bath (135°C) before the addition of *cis*-$Ru^{II}Cl_2$(DMSO)$_4$ (50 mg, 0.103 mmol). The reaction mixture was heated under reflux for 7 h, then a solution of LiCl (90 mg, 2.12 mmol) in water (5 mL) was added. The mixture was allowed to reflux for 18 h. After gradual cooling to room temperature, the precipitate was filtered off. This material was reprecipitated from methanol with 1 M aqueous NH_4PF_6, filtered off, washed with water and dried to give a dark blue solid. Yield: 97 mg (58%). δ_H (500 MHz, CD_3SOCD_3) 10.24 (2 H, d, *J* = 6.0 Hz, C_5H_3N), 9.76 (4 H, d, *J* = 6.6 Hz, C_5H_4N), 9.66 (2 H, s, C_5H_3N), 9.60 (4 H, d, *J* = 6.9 Hz, C_5H_4N), 9.49 (2 H, s, C_5H_3N), 9.15 (4 H, d, *J* = 6.6 Hz, C_5H_4N), 8.88 (4 H, d, *J* = 6.9 Hz, C_5H_4N), 8.76 (2 H, dd, *J* = 6.0, 0.6 Hz, C_5H_3N), 8.35 (4 H, d, *J* = 8.5 Hz, C_6H_4), 8.29 (4 H, d, *J* = 8.8 Hz, C_6H_4), 8.14 (4 H, d, *J* = 8.5 Hz, C_6H_4), 8.07− 8.03 (6 H, C_5H_3N + C_6H_4), 7.93 (2 H, dd, *J* = 6.1, 0.9 Hz,

C_5H_3N). ν(C=O) 1702s cm^{-1}. Anal. Calcd (%) for $C_{68}H_{48}Cl_2F_{24}N_8O_8P_4Ru$: C, 44.0; H, 2.6; N, 6.0. Found: C, 44.0; H, 3.0; N, 5.9.

*2.2.10. cis-[$Ru^{II}(NCS)_2(Me_2qpy^{2+})_2$][$PF_6$]$_4$ (**8**)*

The initial reaction was carried out exactly as for **1**. A solution of KSCN (120 mg, 1.23 mmol) in water (2 mL) was added to the deep blue solution and allowed to reflux for 24 h. After cooling to room temperature, a dark blue precipitate was filtered off, washed with a little *n*-propanol and dried. The solid was dissolved in 1:1 water/methanol (*ca*. 20 mL), and addition of 1 M NH_4PF_6 gave a dark blue precipitate which was filtered off, washed with water and dried. Purification was achieved by using a silica gel column, eluting with 0.3 M NH_4PF_6 in acetonitrile. The first major blue fraction was evaporated to dryness, washed with water and dried to afford a dark blue solid. Yield: 18 mg (22%). δ_H (400 MHz, CD_3CN) 9.67 (2 H, d, J = 6.0 Hz, C_5H_3N), 9.05 (2 H, d, J = 1.5 Hz, C_5H_3N), 8.89−8.86 (6 H, C_5H_4N + C_5H_3N), 8.74 (4 H, d, J = 6.8 Hz, C_5H_4N), 8.60 (4 H, d, J = 6.8 Hz, C_5H_4N), 8.38−8.34 (6 H, C_5H_4N + C_5H_3N), 7.97 (2 H, d, J = 6.0 Hz, C_5H_3N), 7.61 (2 H, dd, J = 5.9, 1.9 Hz, C_5H_3N), 4.42 (6 H, s, Me), 4.33 (6 H, s, Me). ν(C≡N) 2091s cm^{-1}. Anal. Calcd (%) for $C_{46}H_{40}F_{24}N_{10}P_4RuS_2$•$2H_2O$: C, 36.5; H, 2.9; N, 9.3. Found: C, 37.0; H, 2.8; N, 8.8. MALDI-MS: m/z = 1334 ([M − PF_6]$^+$), 1189 ([M − $2PF_6$]$^+$).

All of the compounds **9**–**13** (dark blue solids) were prepared and purified in a manner similar to **8**, from an initial reaction exactly as for the corresponding chloride complex salt, and using a column eluant of 0.05 M NH_4PF_6 in acetonitrile.

*2.2.11. cis-[$Ru^{II}(NCS)_2(Ph_2qpy^{2+})_2$][$PF_6$]$_4$ (**9**)*

Yield: 43 mg (40%). δ_H (400 MHz, CD_3CN) 9.75 (2 H, d, J = 6.0 Hz, C_5H_3N), 9.23–9.20 (6 H, C_5H_4N + C_5H_3N), 9.08 (4 H, d, J = 7.1 Hz, C_5H_4N), 9.04 (2 H, d, J = 2.0 Hz, C_5H_3N), 8.82 (4 H, d, J = 7.1 Hz, C_5H_4N), 8.60 (4 H, d, J = 7.1 Hz, C_5H_4N), 8.47 (2 H, dd, J = 6.0, 2.0 Hz, C_5H_3N), 8.08 (2 H, d, J = 6.3 Hz, C_5H_3N), 7.87−7.81 (10 H, Ph), 7.77–7.73 (12

H, C_5H_3N + Ph). ν(C≡N) 2094s cm^{-1}. Anal. Calcd (%) for $C_{66}H_{48}F_{24}N_{10}P_4RuS_2$•$3.5H_2O$: C, 44.3; H, 3.1; N, 7.8. Found: C, 44.0; H, 2.6; N, 7.6. MALDI-MS: m/z = 1582 ($[M - PF_6]^+$).

*2.2.12. cis-[$Ru^{II}(NCS)_2${(4-AcPh)$_2$qpy^{2+}}$_2$][PF_6]$_4$ (**10**)*

Yield: 36 mg (31%). δ_H (400 MHz, CD_3CN) 9.76 (2 H, d, J = 6.0 Hz, C_5H_3N), 9.25 (4 H, d, J = 7.3 Hz, C_5H_4N), 9.21 (2 H, d, J = 2.0 Hz, C_5H_3N), 9.11 (4 H, d, J = 7.3 Hz, C_5H_4N), 9.05 (2 H, d, J = 1.8 Hz, C_5H_3N), 8.85 (4 H, d, J = 7.3 Hz, C_5H_4N), 8.62 (4 H, d, J = 7.1 Hz, C_5H_4N), 8.48 (2 H, dd, J = 6.0, 2.0 Hz, C_5H_3N), 8.35 (4 H, d, J = 8.8 Hz, C_6H_4), 8.28 (4 H, d, J = 8.8 Hz, C_6H_4), 8.09 (2 H, d, J = 6.0 Hz, C_5H_3N), 7.98 (4 H, d, J = 8.8 Hz, C_6H_4), 7.88 (4 H, d, J = 8.8 Hz, C_6H_4), 7.75 (2 H, dd, J = 6.2, 1.9 Hz, C_5H_3N), 2.72 (6 H, s, Me), 2.68 (6 H, s, Me). ν(C≡N) 2095s, ν(C=O) 1682s cm^{-1}. Anal. Calcd (%) for $C_{74}H_{56}F_{24}N_{10}O_4P_4RuS_2$•$3.5H_2O$: C, 45.4; H, 3.2; N, 7.2. Found: C, 45.3; H, 3.0; N, 7.2. MALDI-MS: m/z = 1750 ($[M - PF_6]^+$).

*2.2.13. cis-[$Ru^{II}(NCS)_2${(2-Pym)$_2$qpy^{2+}}$_2$][PF_6]$_4$ (**11**)*

Yield: 23 mg (23%). δ_H (400 MHz, CD_3CN) 10.23 (4 H, d, J = 7.1 Hz, C_5H_4N), 10.07 (4 H, d, J = 7.3 Hz, C_5H_4N), 9.77 (2 H, d, J = 6.0 Hz, C_5H_3N), 9.23 (2 H, d, J = 1.5 Hz, C_5H_3N), 9.17 (4 H, d, J = 4.8 Hz, $C_4H_3N_2$), 9.10 (4 H, d, J = 4.8 Hz, $C_4H_3N_2$), 9.07 (2 H, d, J = 1.5 Hz, C_5H_3N), 8.89 (4 H, d, J = 7.1 Hz, C_5H_4N), 8.66 (4 H, d, J = 7.3 Hz, C_5H_4N), 8.50 (2 H, dd, J = 5.9, 1.9 Hz, C_5H_3N), 8.09 (2 H, d, J = 5.8 Hz, C_5H_3N), 7.91 (2 H, t, J = 4.8 Hz, $C_4H_3N_2$), 7.85 (2 H, t, J = 4.8 Hz, $C_4H_3N_2$), 7.76 (2 H, dd, J = 6.2, 2.0 Hz, C_5H_3N). ν(C≡N) 2092s cm^{-1}. Anal. Calcd (%) for $C_{58}H_{40}F_{24}N_{18}P_4RuS_2$•$2.5H_2O$: C, 39.2; H, 2.6; N, 14.2. Found: C, 39.2; H, 2.3; N, 13.8. MALDI-MS: m/z = 1589 ($[M - PF_6]^+$), 1444 ($[M - 2PF_6]^+$).

*2.2.14. cis-[$Ru^{II}(NCS)_2${(3,5-MC$_2$Ph)$_2$qpy^{2+}}$_2$][PF_6]$_4$ (**12**)*

Yield: 28 mg (21%). δ_H (400 MHz, CD_3CN) 9.77 (2 H, d, J = 6.0 Hz, C_5H_3N), 9.26 (4 H, d, J = 7.1 Hz, C_5H_4N), 9.22 (2 H, d, J = 1.8 Hz, C_5H_3N), 9.13 (4 H, d, J = 7.3 Hz, C_5H_4N), 9.06 (2 H, d, J = 1.8 Hz, C_5H_3N), 8.89 (2 H, t, J = 1.4 Hz, C_6H_3), 8.87 (4 H, d, J = 7.1 Hz, C_5H_4N), 8.84 (2 H, t, J = 1.5 Hz, C_6H_3), 8.67 (4 H, d, J = 1.5 Hz, C_6H_3), 8.64 (4 H, d,

J = 7.6 Hz, C_5H_4N), 8.57 (4 H, d, *J* = 1.3 Hz, C_6H_3), 8.49 (2 H, dd, *J* = 6.0, 2.0 Hz, C_5H_3N), 8.10 (2 H, d, *J* = 6.0 Hz, C_5H_3N), 7.76 (2 H, dd, *J* = 6.3, 2.0 Hz, C_5H_3N), 4.02 (12 H, s, Me), 3.98 (12 H, s, Me). *ν*(C≡N) 2091s, *ν*(C=O) 1720s cm^{-1}. Anal. Calcd (%) for $C_{82}H_{64}F_{24}N_{10}O_{16}P_4RuS_2 \bullet 3H_2O$: C, 43.9; H, 3.1; N, 6.2. Found: C, 44.0; H, 2.8; N, 6.3. MALDI-MS: *m*/*z* = 2046 ($[M - PF_6]^+$).

*2.2.15. cis-[Ru^{II}(NCS)$_2${(4-MCPh)$_2$qpy^{2+}}$_2$][PF$_6$]$_4$ (**13**)*

Yield: 34 mg (30%). δ_H (400 MHz, CD_3CN) 9.76 (2 H, d, *J* = 6.0 Hz, C_5H_3N), 9.23 (4 H, d, *J* = 7.1 Hz, C_5H_4N), 9.21 (2 H, d, *J* = 1.8 Hz, C_5H_3N), 9.09 (4 H, d, *J* = 7.1 Hz, C_5H_4N), 9.05 (2 H, d, *J* = 1.8 Hz, C_5H_3N), 8.85 (4 H, d, *J* = 7.3 Hz, C_5H_4N), 8.62 (4 H, d, *J* = 7.3 Hz, C_5H_4N), 8.47 (2 H, dd, *J* = 6.2, 1.9 Hz, C_5H_3N), 8.39 (4 H, d, *J* = 8.8 Hz, C_6H_4), 8.33 (4 H, d, *J* = 8.8 Hz, C_6H_4), 8.09 (2 H, d, *J* = 6.0 Hz, C_5H_3N), 7.96 (4 H, d, *J* = 8.8 Hz, C_6H_4), 7.87 (4 H, d, *J* = 8.8 Hz, C_6H_4), 7.75 (2 H, dd, *J* = 6.3, 2.0 Hz, C_5H_3N), 3.98 (6 H, s, Me), 3.95 (6 H, s, Me). δ_H (500 MHz, CD_3SOCD_3) 9.80 (4 H, d, *J* = 6.6 Hz, C_5H_4N), 9.73 (2 H, s, C_5H_3N), 9.65 (4 H, d, *J* = 6.9 Hz, C_5H_4N), 9.61 (2 H, d, *J* = 5.7 Hz, C_5H_3N), 9.57 (2 H, s, C_5H_3N), 9.15 (4 H, d, *J* = 6.6 Hz, C_5H_4N), 8.92− 8.89 (6 H, C_5H_4N + C_5H_3N), 8.39 (4 H, d, *J* = 8.2 Hz, C_6H_4), 8.33 (4 H, d, *J* = 8.8 Hz, C_6H_4), 8.19 (4 H, d, *J* = 8.5 Hz, C_6H_4), 8.15 (2 H, d, *J* = 6.0 Hz, C_5H_3N), 8.09 (4 H, d, *J* = 8.8 Hz, C_6H_4), 8.02 (2 H, d, *J* = 6.3 Hz, C_5H_3N), 3.98 (6 H, s, Me), 3.94 (6 H, s, Me). *ν*(C≡N) 2095s, *ν*(C=O) 1717s cm^{-1}. Anal. Calcd (%) for $C_{74}H_{56}F_{24}N_{10}O_8P_4RuS_2 \bullet 3H_2O$: C, 44.2; H, 3.1; N, 7.0. Found: C, 44.0; H, 2.9; N, 6.9. MALDI-MS: *m*/*z* = 1813 ($[M - PF_6]^+$), 1669 ($[M - 2PF_6]^+$).

*2.2.16. cis-[Ru^{II}(NCS)$_2${[4-(CO$_2$H)Ph]$_2$qpy^{2+}}$_2$][PF$_6$]$_4$ (**14**)*

A portion of crude *cis*-$[Ru^{II}Cl_2\{[4\text{-}(CO_2H)Ph]_2qpy^{2+}\}_2]Cl_4$ was prepared exactly as described above for **7**. The solid was added to 2-methoxyethanol (25 mL) and heated to reflux before addition of KSCN (202 mg, 2.08 mmol) in water (5 mL). The mixture was left to reflux for 24 h. After partially cooling, solid NH_4PF_6 (*ca*. 1 g) was added to the warm solution and the volume was reduced under vacuum. Water (20 mL) was added to afford a dark blue precipitate which was filtered off, washed with water and dried. Yield: 94 mg

(55%). δ_H (500 MHz, CD_3SOCD_3) 9.79 (4 H, d, J = 6.6 Hz, C_5H_4N), 9.74 (2 H, s, C_5H_3N), 9.64 (4 H, d, J = 6.9 Hz, C_5H_4N), 9.61 (2 H, d, J = 6.0 Hz, C_5H_3N), 9.58 (2 H, s, C_5H_3N), 9.16 (4 H, d, J = 6.9 Hz, C_5H_4N), 8.92– 8.89 (6 H, C_5H_4N + C_5H_3N), 8.35 (4 H, d, J = 8.2 Hz, C_6H_4), 8.29 (4 H, d, J = 8.5 Hz, C_6H_4), 8.16– 8.14 (6 H, C_5H_3N + C_6H_4), 8.05– 8.02 (6 H, C_5H_3N + C_6H_4). ν(C≡N) 2091s, ν(C=O) 1701s cm^{-1}. Anal. Calcd (%) for $C_{70}H_{48}F_{24}N_{10}O_8P_4RuS_2$: C, 44.2; H, 2.5; N, 7.4. Found: C, 44.2; H, 2.6; N, 6.9.

2.3. X-ray crystallography

Crystals of $[(4\text{-}(CO_2H)Ph)_2qpyH^{3+}][HSO_4]_3 \bullet 3H_2O$ were grown by very slow evaporation of a concentrated filtrate solution containing a mixture of *tert*-butanol, H_2SO_4 and water. This filtrate was collected from several syntheses of $[(4\text{-}(CO_2H)Ph)_2qpy^{2+}]Cl_2$, and allowed to stand in a fume-cupboard for a few weeks. A crystal from this filtrate was selected at random. Data were collected on a Bruker APEX II CCD X-ray diffractometer by using MoK_α radiation (λ = 0.71073 Å), and the data were processed by using the Bruker SAINT [13] and SADABS [14] software packages. The structure was solved by direct methods by using SHELXS-97 [15], and refined by full-matrix least-squares on all F_0^2 data by using SHELXL-97 [16]. The asymmetric unit contains one trication with the atom N2 protonated, three HSO_4^- anions and three water molecules. All non-hydrogen atoms were refined anisotropically and most of the hydrogen atoms (except those bonded to N2, and in the water molecules and anions) were included in idealised positions by using the 'riding model', with thermal parameters of 1.2 times those of aromatic parent carbon atoms, and 1.5 times those of methyl parent carbons. All other calculations were carried out by using the SHELXTL package [17]. Crystallographic data and refinement details are presented in Table 1.

Table 1

Crystallographic data and refinement details for the salt [(4-$(CO_2H)Ph)_2qpyH^{3+}$][HSO_4]$_3$•3H_2O

Formula	$C_{34}H_{34}N_4O_{19}S_3$
Molecular weight	898.83
Crystal system	Triclinic
Space group	$P\bar{1}$
a (Å)	10.3525 (16)
b (Å)	10.7378 (17)
c (Å)	18.030 (3)
α (°)	99.452 (3)
β (°)	90.168 (3)
γ (°)	113.477 (2)
U (Å^3)	1808.2 (5)
Z	2
D_{calcd} (Mg m^{-3})	1.651
T (K)	100 (2)
μ (mm^{-1})	0.299
Crystal size (mm)	0.45 × 0.30 × 0.25
Crystal appearance	yellow block
Reflections collected	10590
Independent reflections (R_{int})	7230 (0.0234)
θ_{max}/° (completeness)	26.43 (97.3%)
Reflections with $I > 2\sigma(I)$	6621
Goodness-of-fit on F^2	1.075
Final $R1$, $wR2$ [$I > 2\sigma(I)$]	0.0417, 0.1070
(all data)	0.0458, 0.1101
Peak and hole (eÅ^{-3})	0.467, − 0.342

2.4. Theoretical calculations

Density functional theory (DFT) and time-dependent DFT (TD-DFT) calculations were carried out by using the Gaussian 03 software package [18]. The structures were optimised at the BP86 [19,20] level by using the Def2-SV(P) [21] basis set, with inclusion of a conductor-like polarizable continuum model (CPCM) [22,23] to take into account the solvent effect of DMSO for the complex in salt **14** (denoted **14′**). The TD-DFT calculations on the complex in salt **7** (denoted **7′**) were performed at the MPW1PW91 [24]/Def2-SV(P) level with inclusion of a DMSO CPCM. The TD-DFT calculations on **14′** were also performed by using the MPW1PW91 functional and with a DMSO CPCM, but using the

larger DGDZVP [25] basis set. The first 50 excited states were calculated in each case and UV–vis spectra were simulated by using the GaussSum program [26].

2.5. Fabrication of dye-sensitized solar cells

TiO_2-based cells were fabricated as follows. Fluorine-doped tin oxide (FTO) glass (TEC15, Hartford Glass) was cleaned by successive sonication for 15 min in aqueous detergent, acetone, isopropanol and ethanol. A thin compact layer (60 nm) of TiO_2 was then deposited on the cleaned FTO by spray pyrolysis. The mesoporous layers were prepared by doctor-blading a commercial TiO_2 paste (Dyesol, DSL-18-NR) onto the coated FTO substrates. The film was dried at 80 °C on a hotplate for 15 min and then sintered at 500 °C for 30 min to burn out the organic binder, leaving the mesosporous anatase structure of thickness around 13 μm. After cooling to about 100 °C, the films were immersed into 5×10^{-4} M solutions of the test dyes in DMSO and left for 16 h. Chenodeoxycholic acid (10^{-3} M) was added to the dye bath to reduce dye aggregation on the TiO_2 film. The dye-coated film was washed thoroughly with HPLC grade DMSO and then dried under N_2. The cells were assembled by sealing the dye-coated electrodes to thermally platinized FTO (TEC8) counter electrodes by using a 25 μm thermoplastic gasket (Surlyn) at 80 °C under pressure. The narrow gap between the two electrodes was vacuum filled with electrolyte via holes predrilled in the counter electrode. The filling holes were sealed with microscope slip by using Surlyn. For complex salts **7** and **14**, the electrolyte was composed of 0.06 M I_2, 0.6 M 1-propyl-3-methylimidazolium iodide (PMII), 0.5 M LiI, 0.1 M guanidinium thiocyanate (GuSCN) and 0.5 M *tert*-butylpyridine (TBP) in 3-methoxypropionitrile (MPN). For the N719 reference, the electrolyte was composed of 0.05 M I_2, 0.6 M PMII, 0.2 M NaI, 0.1 M GuSCN and 0.1 M *N*-methylbenzimidazole in MPN. All of the chemicals used in the cell fabrication were obtained from Sigma-Aldrich. The active area of the cells was 0.5 cm^2.

ZnO-based cells were fabricated as follows. The ZnO paste was prepared by using a 1:1 mixture of two commercial ZnO powders, Evonik VP AdNano@ZnO20 (particle size *ca*. 20 nm) and PI-KEM (particle size *ca*. 50 nm). For thin film preparation, the mixture was

dispersed in water and ethanol (30:70) and stirred overnight to obtain a colloidal suspension of 30 wt %. This suspension was spread onto previously cleaned FTO glass with a glass rod by using Scotch tape as spacer, and the film was then heated at 420 °C for 30 min. The ZnO substrates were coated with the test dyes in similar manner to the TiO_2 films, except that the immersion time was only 1 h. The counter electrode was prepared by spreading 15 μl of *platisol* (Solaronix) on the conductive side of TEC8 electrodes and subsequent annealing at 400 °C for 5 min. Cells were assembled exactly as those containing the TiO_2 films.

Three different electrolyte solutions were tested in the ZnO-based cells with the complex salt **14**: (1) 0.5 M LiI, 0.05 M I_2, 0.5 M TBP in MPN; (2) 0.5 M LiI, 0.03 M I_2, 0.5 M TBP, 0.1 M GuSCN in acetonitrile; (3) 0.03 M I_2, 0.6 M PMII, 0.1 M GuSCN, 0.5 M TBP in acetonitrile. Electrolyte 3 gave the best cell performance, so data were obtained for **7** in this electrolyte only. The active area of the cells was 0.81 cm^2.

2.6. Current-voltage measurements

The current-voltage characteristics of the TiO_2-based cells were measured using a solar simulator (Müller) equipped with 1 kW xenon lamp. The intensity of the illumination was calibrated with a standard silicon reference cell (Fraunhofer ISE) to provide 1 sun (100 mW cm^{-2}). AM 1.5 and KG5 filters were used to minimize the mismatch between the solar simulator and the AM 1.5 solar spectrum. The current voltage plots were recorded by using a computer-controlled system (Whistonbrook).

The ZnO-based cells were characterised with a solar simulator (ABET) combined with a AM 1.5G filter. A reference cell with temperature output (Oriel, 91150) was used for calibrate the illumination output to 1 sun. Photocurrents, photovoltages and current-voltage curves were measured by using a 2400 Keithley SourceMeter.

3. Results and discussion

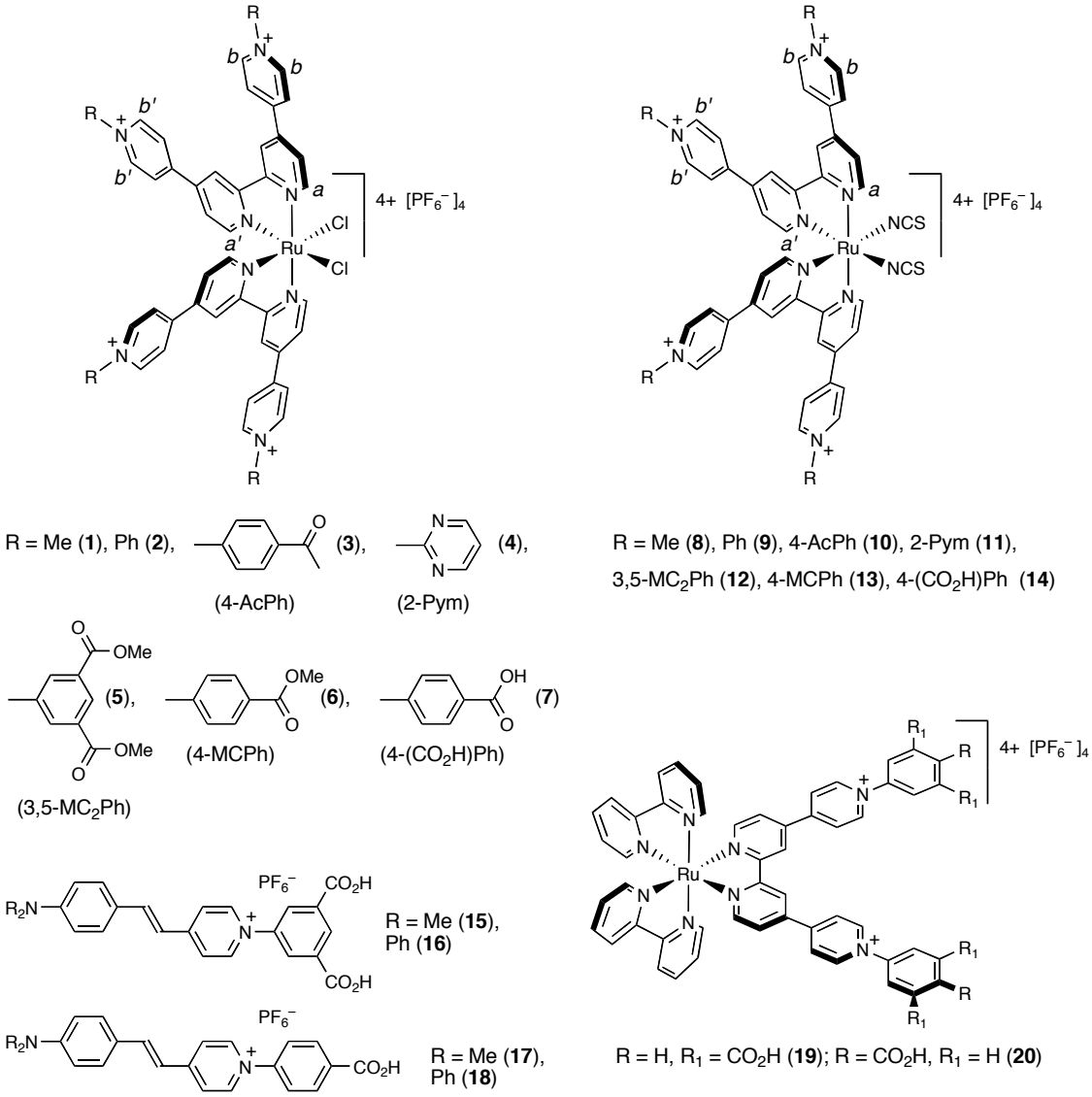

Fig. 1. Chemical structures of the Ru^{II} complex salts investigated, including the labeling for selected protons for which the ^1H NMR chemical shifts are discussed. The structures of previously studied acid-finctionalised stilbazolium and complex salts are also shown [9,11].

3.1. Synthesis and characterisation

We have investigated previously Ru^{II} complex salts of R_2qpy^{2+} ligands, largely for their interesting NLO properties [4–6]. More recently, we studied also species with a *cis*-

$\{Ru^{II}(2,2'\text{-bpy})_2\}^{2+}$ moiety coordinated to two such ligands (*e.g.* **19** and **20**, Fig. 1) [11], and the photosensitizer stilbazolium salts **15**–**18** [9]. The new complexes in salts **1**–**14** (Fig. 1) were prepared partly to compare their optical and redox properties with these related known species, but also to assess the photosensitizing abilities of **7** and **14**.

Attempts at preparing the new proligand salts $[(3,5\text{-}(CO_2H)_2Ph)_2qpy^{2+}]Cl_2$ and $[(4\text{-}(CO_2H)Ph)_2qpy^{2+}]Cl_2$ via base-catalysed hydrolysis of their corresponding known methyl esters [5,11] were unsuccessful. The production of insoluble brown materials indicated decomposition reactions, probably due to nucleophilic attack by hydroxide anions on the pyridinium rings. Because acid-catalysed ester hydrolysis requires more electron-donating alkyl groups on the ester, transesterifications with *tert*-butanol and a catalytic amount of conc. H_2SO_4 were attempted. However, instead of producing *tert*-butyl esters, these reactions afforded the desired carboxylic acid derivatives cleanly and in high yields.

The dichloro complexes in **1**–**6** were synthesised from the precursor *cis*-$Ru^{II}Cl_2(DMSO)_4$ with a little under two equivalents of the appropriate $[R_2qpy^{2+}]Cl_2$ salt in refluxing *n*-propanol. Subsequent prolonged treatment with an excess of aqueous LiCl gave the Cl^- salts of the complexes as dark blue precipitates, which were metathesised to their PF_6^- salts. Relatively good yields in the range ca. 60–70% were obtained. It is noteworthy that using lower reaction temperatures (with ethanol as the solvent), shorter reaction times, and/or avoiding the LiCl treatment consistently gave impure products that could not be purified by reprecipitation or various column chromatographic approaches. The carboxylic acid-functionalised complex salt **7** was prepared by using a method similar to that for **1**–**6**, but with 2-methoxyethanol as the initial solvent to give a higher reaction temperature necessary to dissolve the proligand salt. Attempts at preparing **7** by ester hydrolysis of **6** under either basic or acidic conditions lead to decomposition only, necessitating the use of the pre-hydrolysed proligand salt. Unfortunately, $[(3,5\text{-}MC_2Ph)_2qpy^{2+}]Cl_2$ is insufficiently soluble in appropriate solvents to allow effective complexation reactions.

The dithiocyanato complexes in **8**–**13** were prepared via their dichloro counterparts formed *in situ*, as in previous reports of neutral complexes [27]. Column chromatography on silica gel was used to purify these products as their PF_6^- salts, giving moderate yields of *ca.*

20–40%. Even after chromatography, there are still minor peaks in the ^{1}H NMR spectra for all of **8**–**13**. Subsequent reprecipitations and anion metatheses did not remove these minor signals; these change with the ligand, but are always present at higher field with respect to the main product peaks, so cannot be chloro species. Also, any traces of unreacted proligand are removed by column chromatography. Because thiocyanate is an ambidentate ligand, N/S linkage isomerism is possible, making it difficult to separate the isomers by column chromatography. Ru^{II} thiocyanate linkage isomers have been studied in several instances [28]. Recently, X-ray crystal structures of both isomers have been obtained by Vandenburgh et al. for $[Ru^{II}(2,2'\text{-bpy})(\eta^6\text{-}para\text{-cymene})(NCS)]PF_6$ [28e], and by Brewster et al. for $[Ru^{II}(4,4'\text{-}^tBu_2\text{-}2,2'\text{-bpy})(tpy)(NCS)]SbF_6$ [28f]. Interestingly, the relative positions of ^{1}H NMR signals corresponding to the S-bound and N-bound isomers depend on the particular molecular structure.

Again, due to solubility considerations, the use of 2-methoxyethanol was necessary in order to access the carboxylic acid-functionalised complex salt **14**. The reaction mixture was cooled only partially before adding excess NH_4PF_6, to prevent the complex from precipitating out as its NCS^- salt. Notably, the solubilities of both **14** and **7** are poor, and appreciable in DMSO only. The identities and purities of all the new complex salts are confirmed by diagnostic ^{1}H NMR spectra, together with +electrospray or MALDI mass spectra for all except **7** and **14**. IR spectra provide further characterisation data when ester, carboxylic acid or thiocyanate groups are present. CHN elemental analyses all fit satisfactorily for variable levels of hydration, typically observed for organic salts. This residual water resists drying under vacuum at room temperature (the samples were not heated in order to avoid any possible decomposition).

3.2. ^{1}H NMR spectroscopy

^{1}H NMR spectra were recorded in CD_3CN for complex salts **1**–**6** and **8**–**13**. All show two sets of signals in the aromatic region, confirming their cis coordination geometry. Appropriate numbers of singlet signals due to methyl groups are also observed at higher field.

Table 2 includes selected data, while Fig. 2 shows a fully assigned spectrum for **8**. The signal assignments were based on splitting patterns and *J* values, allowing unambiguous identification of the environments within the individual 4,4′-bipyridyl (4,4′-bpy) units, with the only uncertainty relating to the *e*,*e*′/*d*,*d*′ protons. However, the lowest field four proton doublet ($J \approx 7.0$ Hz) signals are almost certainly due to the protons *e*,*e*′ that are adjacent to the deshielding quaternised N atoms [11]. The assignments are reinforced by making comparisons with the spectra of related complexes, aided by COSY data.

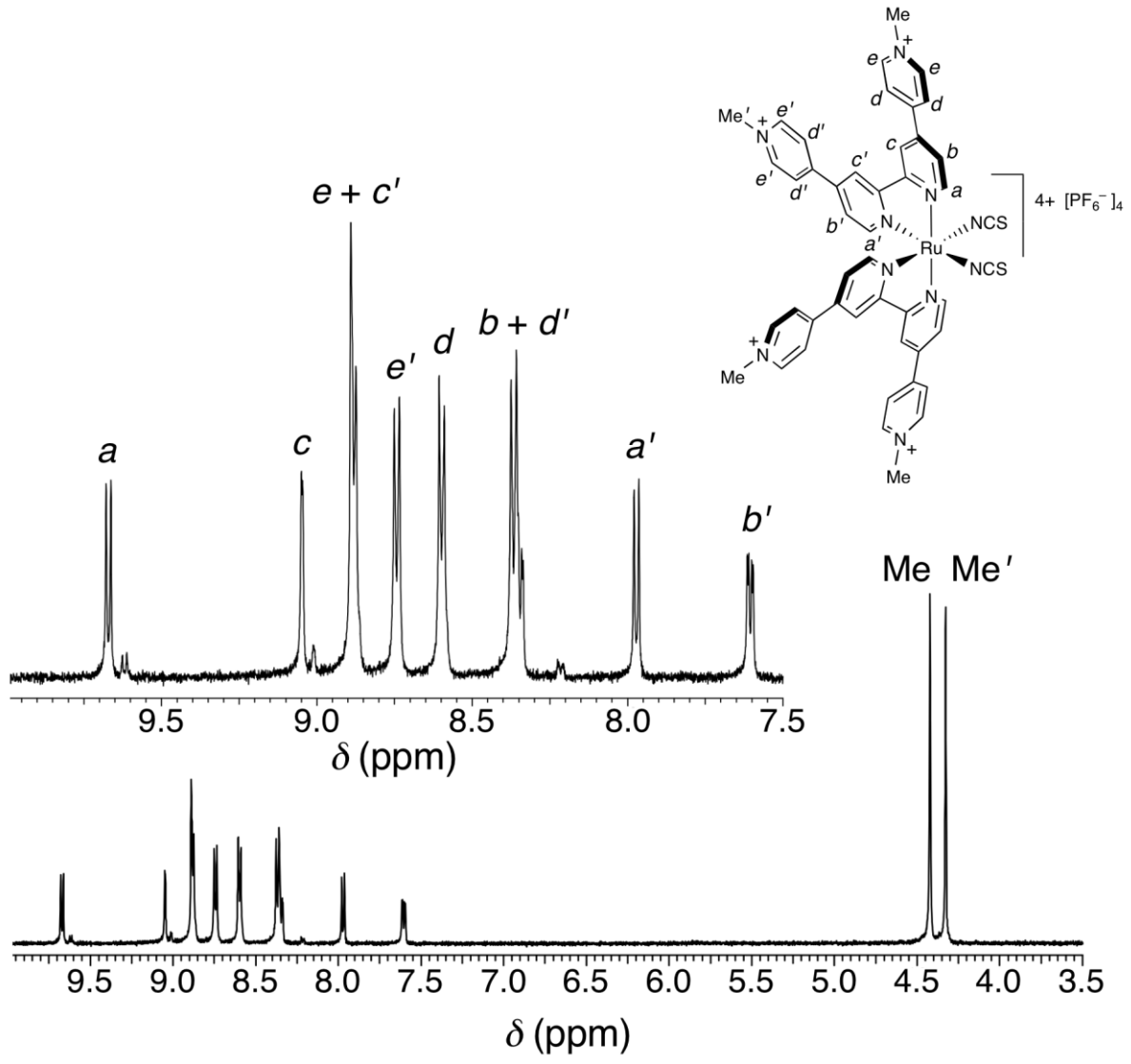

Fig. 2. ^{1}H NMR spectrum of **8** recorded at 400 MHz in CD_3CN at 293 K.

It is reasonable to assume that the protons in the 4,4′-bpy units that are positioned trans relative to the Cl^- or NCS^- ligands are more shielded, and therefore shifted upfield when compared to the others that are mutually trans. It is worth comparing the doublet ($J \approx$ 6.0 Hz) signals corresponding to the protons in the 6,6′-positions of the 2,2′-bpy ring (*a* and *a′*). The separation between these signals is much greater for the dichloro species, because Cl^- is more shielding than NCS^-, due to its higher electronegativity.

The protons *e* and *e′* are sensitive to the R substituent, as expected. Downfield shifts of *ca*. 1.3 ppm are observed on moving from **1** to **4** and from **8** to **11**, as the pyridinium group becomes more electron deficient. Based on the chemical shifts of these signals, the electron-withdrawing strength of R in both series of complex salts is Me < Ph ≤ 4-MCPh ≤ 4-AcPh ≤ 3,5-MC_2Ph < 2-Pym, similar to that observed for the *cis*-$[Ru^{II}(2,2'\text{-bpy})_2(R_2qpy^{2+})][PF_6]_4$ compounds reported previously [11].

Table 2

Selected ^{1}H NMR data for complex salts **1**–**6** and **8**–**13** recorded in CD_3CN at 400 MHz.

complex salt	δ (ppm)			
	a	*a′*	*e*	*e′*
1	10.29	7.94	8.86	8.71
2	10.34	8.03	9.20	9.05
3	10.35	8.05	*ca*. 9.23[a]	*ca*. 9.08[a]
4	10.41	8.02	10.22	10.05
5	10.37	8.04	*ca*. 9.25[a]	9.11
6	10.34	8.04	*ca*. 9.22[a]	*ca*. 9.06[a]
8	9.67	7.97	*ca*. 8.88[a]	8.74
9	9.75	8.08	*ca*. 9.21[a]	9.08
10	9.76	8.09	9.25	9.11
11	9.77	8.09	10.23	10.07
12	9.77	8.10	9.26	9.13
13	9.76	8.09	9.23	9.09

[a] Overlapped with another signal.

Due to insolubility in CD_3CN, the spectra of **7** and **14** could be recorded in CD_3SOCD_3 only, so the spectra of **6** and **13** were obtained also in CD_3SOCD_3. Comparing the spectra of **6**/**7** and **13**/**14**, the doublet signals corresponding to the phenyl protons are shifted upfield only slightly on changing from an ester to a carboxylic acid substituent.

3.3. Electronic spectroscopy

UV–vis absorption data for **1**–**6** and **8**–**13** measured in acetonitrile, and for **7** and **14** in DMSO are presented in Table 3. Representative spectra are shown in Figs. 3–5.

Table 3

UV–vis absorption and electrochemical data for the complex salts **1**–**14**.

compound	λ_{max}, nm (ε, 10^3 M^{-1} cm^{-1})[a]	E_{max}, eV	assignment	$E_{1/2}$ or E, V vs. Ag–AgCl (ΔE_p, mV)[b]	
				$Ru^{III/II}$	reductions
1	616 (23.6)	2.01	d → π*	0.66 (80)	–0.66[c]
	509 (20.8)	2.44	d → π*		–0.87[d]
	261 (90.1)	4.75	π → π*		–1.26[c]
2	636 (33.4)	1.95	d → π*	0.68 (70)	–0.53[c]
	535 (23.7)	2.32	d → π*		–0.69[d]
	278 (76.2)	4.46	π → π*		–1.22[c]
					–1.39[c]
3	640 (30.6)	1.94	d → π*	0.70 (70)	–0.39[c]
	538 (22.6)	2.30	d → π*		–0.51[d]
	290 (87.8)	4.27	π → π*		–1.08[c]
					–1.24[c]
4	655 (29.8)	1.89	d → π*	0.71 (80)	–0.20[c]
	553 (24.2)	2.24	d → π*		–0.35[d]
	284 (106.0)	4.37	π → π*		–1.04[c]
					–1.24[c]
5	643 (36.2)	1.93	d → π*	0.70 (70)	–0.41[c]
	540 (25.6)	2.30	d → π*		–0.57[d]
	279 (100.9)	4.44	π → π*		–1.14[c]
					–1.32[c]
6	643 (31.1)	1.93	d → π*	0.70 (70)	–0.35[c]
	540 (23.0)	2.30	d → π*		–0.53[d]
	286 (90.4)	4.33	π → π*		–1.09[c]
					–1.25[c]
7	650 (23.8)	1.91	d → π*		
	545 (14.3)	2.27	d → π*		
	286 (61.7)	4.33	π → π*		
8	576 (22.5)	2.15	d → π*	0.92 (90)	–0.62[c]
	480 (19.8)	2.58	d → π*		–0.84[d]
	256 (86.3)	4.84	π → π*		–1.38[c]
9	584 (25.3)	2.12	d → π*	0.92 (110)	–0.45[c]
	492 (21.6)	2.52	d → π*		–0.60[d]
	274 (66.9)	4.52	π → π*		–1.12[c]
					–1.27[c]
10	591 (27.6)	2.10	d → π*	0.92 (120)	–0.36[c]

	497 (22.5)	2.49	d → π*		–0.48[d]
	285 (85.7)	4.35	π → π*		–1.01[c]
					–1.13[c]
11	606 (28.6)	2.05	d → π*	0.93 (120)	–0.16[c]
	513 (20.6)	2.42	d → π*		–0.32[d]
	280 (101.7)	4.43	π → π*		–0.94[c]
					–1.11[c]
12	593 (25.7)	2.09	d → π*	0.92 (120)	–0.36[c]
	498 (20.1)	2.49	d → π*		–0.51[d]
	276 (88.5)	4.49	π → π*		–1.03[c]
					–1.18[c]
13	593 (25.1)	2.09	d → π*	0.91 (120)	–0.33[c]
	498 (19.7)	2.49	d → π*		–0.51[d]
	283 (77.0)	4.38	π → π*		–1.01[c]
					–1.14[c]
14	602 (20.8)	2.06	d → π*		
	507 (13.5)	2.44	d → π*		
	285 (62.1)	4.35	π → π*		
N3	544 (14.2)	2.28	d → π*		
	403 (13.7)	3.08	d → π*		
	319 (43.9)	3.89	π → π*		

[a] Solutions *ca*. 2×10^{-5} M for **1**–**14**, all in acetonitrile, except **7** and **14** in DMSO; solution *ca*. 6×10^{-5} M for N3 (*cis*-$Ru^{II}(NCS)_2(4,4'\text{-}(CO_2H)_2\text{-}2,2'\text{-bpy})_2$; first reported by Grätzel and colleagues [29]).

[b] Solutions *ca*. 10^{-3} M in analyte and 0.1 M in $[NBu^n_4]PF_6$ with a scan rate of 200 mV s^{-1} using a glassy carbon working electrode. Ferrocene internal reference $E_{½} = 0.43$ V, $\Delta E_p = 70$ mV.

[c] E_{pa} for an irreversible oxidation process.

[d] E_{pc} for an irreversible reduction process.

The UV–vis spectra of all the new complex salts feature an intense π → π* absorption in the UV region and also two overlapped visible MLCT bands. The low energy (LE) MLCT band is more intense and hence generally more distinct than its counterpart to high energy (HE). The related complexes $[Ru^{II}(R_2qpy^{2+})_3]^{8+}$ also show two resolved bands, and both experimental trends and DFT calculations show that these arise from MLCT to the 2,2′-bpy and pyridinium groups, with the latter transitions corresponding to the HE bands [5]. A

similar pattern is observed also for **1**–**6** and **8**–**13**; the E_{max} value for the LE band varies by only *ca*. 0.1 eV when R is changed, while the HE band E_{max} varies by up to 0.2 eV.

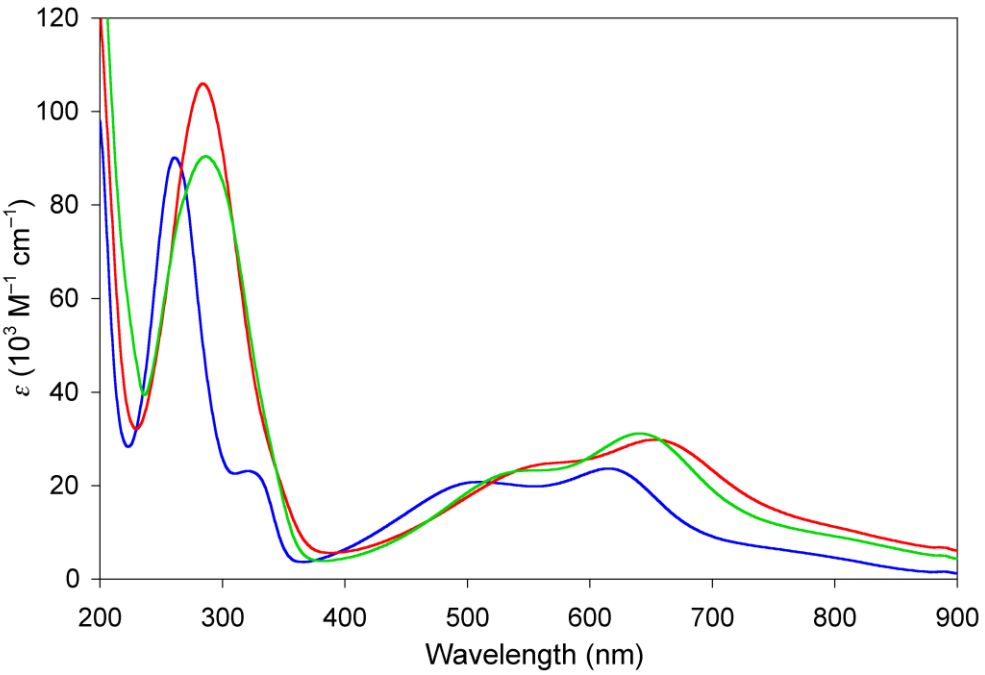

Fig. 3. UV–vis absorption spectra of the complex salts **1** (blue), **4** (red) and **6** (green) in acetonitrile at 293 K.

Within the dichloro (**1**–**6**) and dithiocyanato (**8**–**13**) series, the energies of both MLCT bands decrease as the acceptor strength of the substituent on the R_2qpy^{2+} ligand increases (Figs. 3 and 4). Based on these energies, the electron-withdrawing strength of R in both series is Me < Ph ≤ 4-AcPh ≤ 4-MCPh = 3,5-MC_2Ph < 2-Pym, similar to that indicated by the ^{1}H NMR data (see above). The same general trend is observed also for *cis*-[Ru^{II}(2,2′-bpy)$_2$(R_2qpy^{2+})]$^{4+}$ complexes [11] and other Ru^{II}-R_2qpy^{2+} species [4,5]. However, these new *cis*-[$Ru^{II}X_2$(R_2qpy^{2+})$_2$]$^{4+}$ complexes exhibit substantially red-shifted MLCT bands when compared with the *cis*-[Ru^{II}(2,2′-bpy)$_2$(R_2qpy^{2+})]$^{4+}$ chromophores. This difference is due to the electron-donating Cl^- or NCS^- ligands which destabilise the Ru-based HOMOs. On replacing Cl^- with NCS^-, blue-shifts of *ca*. 0.2 eV are observed for both the MLCT bands (Fig. 5), in keeping with the expected stronger electron-donating ability of Cl^-.

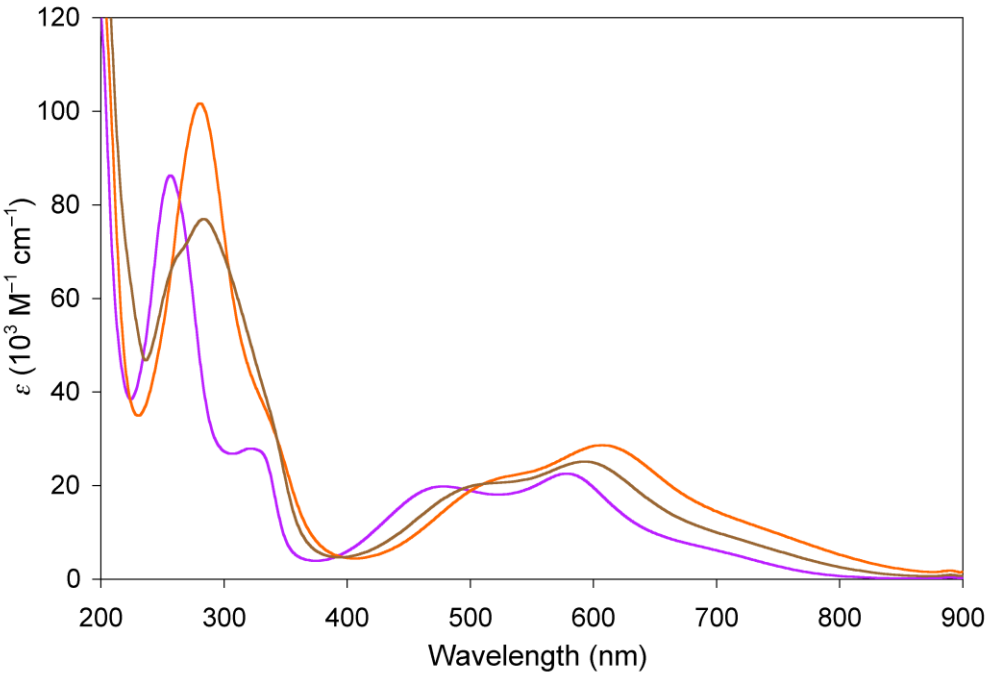

Fig. 4. UV–vis absorption spectra of the complex salts **8** (purple), **11** (orange) and **13** (brown) in acetonitrile at 293 K.

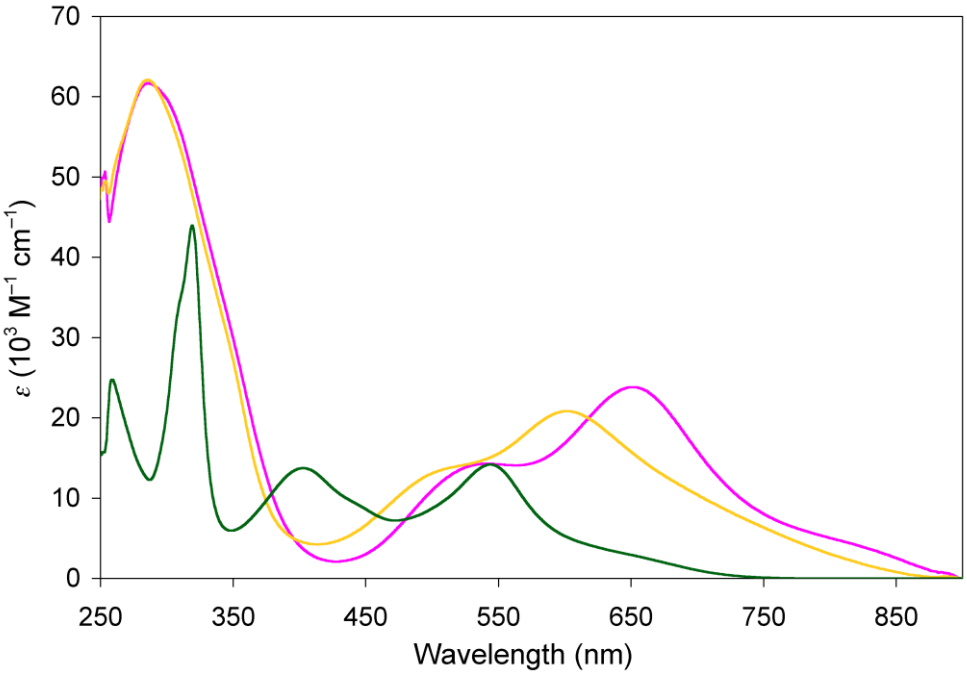

Fig. 5. UV–vis absorption spectra of **7** (magenta), **14** (gold) and N3 (dark green) in DMSO at 293 K.

As in acetonitrile, changing the ancillary ligand from Cl^- to NCS^- increases the energies of both MLCT bands by *ca*. 0.2 eV in DMSO (Fig. 5). Similar behaviour is observed also for the complexes *cis*-$Ru^{II}X_2$(4,4′-$(CO_2Et)_2$-2,2′-bpy)$_2$ (X = Cl^- or NCS^-) in the same solvent [30]. More importantly, the MLCT bands of **7** and **14** are significantly red-shifted and more intense when compared to those of N3 (Fig. 5). The absorption of these new dyes covers the entire visible region (400–700 nm) and extends well into the near-IR (> 750 nm). Thus, incorporating pyridinium-substituted ligands significantly improves the absorption behaviour, an aspect potentially beneficial for DSSC applications.

3.4. Electrochemistry

Cyclic voltammetric data for **1**–**6** and **8**–**13** in acetonitrile are shown in Table 4, and representative voltammograms in Fig. 6. All of the complexes show quasi-reversible or reversible $Ru^{III/II}$ oxidation waves, together with irreversible ligand-based reductions.

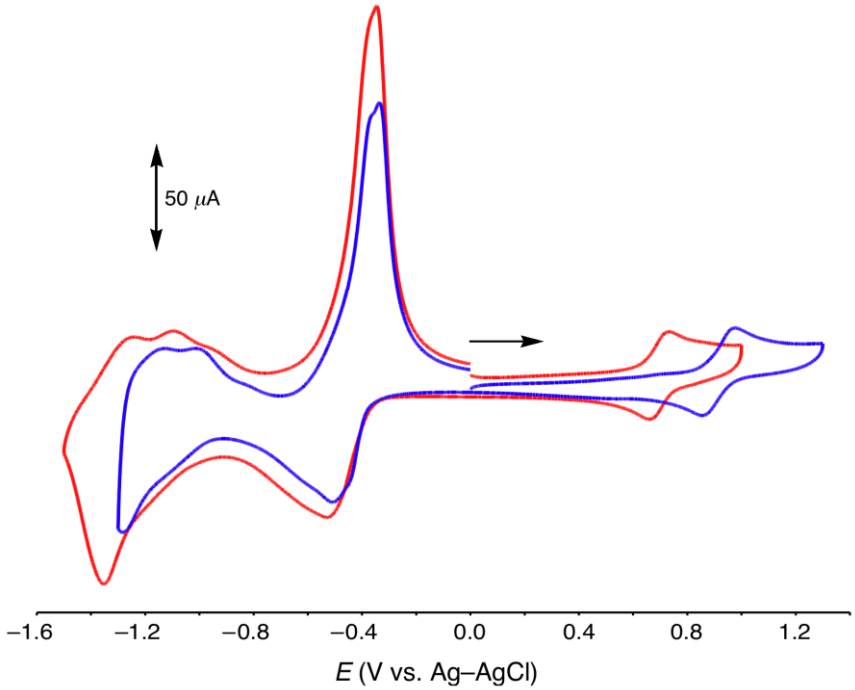

Fig. 6. Cyclic voltammograms for the complex salts **6** (red) and **13** (blue) recorded at 200 mV s^{-1} in acetonitrile (the arrow indicates the direction of the initial scans).

Within the dichloro (**1**–**6**) or dithiocyanato (**8**–**13**) series, the $Ru^{III/II}$ potentials vary only slightly, showing minimal influence of the R group. Similar behaviour is shown by the *cis*-$[Ru^{II}(2,2'\text{-bpy})_2(R_2qpy^{2+})]^{4+}$ complexes [11]. However, the $Ru^{III/II}$ $E_{½}$ values increase by 210–260 mV on changing the ancillary ligand from Cl^- to NCS^- (Fig. 6). For *cis*-$Ru^{II}X_2(4,4'\text{-}(CO_2Et)_2\text{-}2,2'\text{-bpy})_2$ (X = Cl^- or NCS^-) in acetonitrile, a slightly larger difference (290 mV) is observed [31]. These observations clearly indicate that Cl^- is the stronger electron donor, rendering the Ru^{II} centre more electron rich and therefore destabilising the HOMO. This factor is reflected also in the lower MLCT energies observed for the dichloro species in comparison to their dithiocyanato analogues (see above).

As observed also for most of the *cis*-$[Ru^{II}(2,2'\text{-bpy})_2(R_2qpy^{2+})]^{4+}$ complexes [11], **1**–**6** and **8**–**13** show generally poorly defined ligand-based reductive behaviour (Fig. 6). However, the potentials vary significantly on changing the pyridinium substituent. As expected, on moving from an electron-donating Me to an electron-withdrawing 2-Pym group, the E_{pa} value of the first reduction process increases significantly (by 460 mV) in both series. The trend observed with respect to increasing acceptor strength of the pyridinium unit is similar to that for the *cis*-$[Ru^{II}(2,2'\text{-bpy})_2(R_2qpy^{2+})]^{4+}$ complexes [11], and is reflected in the red-shifting of the MLCT bands (see above).

3.5. Crystallography

A single-crystal X-ray structure of the serendipitously obtained compound $[(4\text{-}(CO_2H)Ph)_2qpyH^{3+}][HSO_4]_3 \bullet 3H_2O$ was determined. A representation of the molecular structure is shown in Fig. 7, and crystallographic data and refinement details are summarised in Table 1.

One of the pyridyl nitrogens is protonated due to the high concentration of H_2SO_4 in the filtrates, while the HSO_4^- anions derive from deprotonation of this acid. This *N*-protonation encourages the adoption of a cis conformation, due to some stabilisation by a weak intramolecular N–H•••H hydrogen bond. This conformation is observed in various other structures containing monoprotonated 2,2′-bpy units [32]. In contrast, trans forms are

observed crystallographically for $[Ph_2qpy^{2+}][PF_6]_2 \bullet Me_2CO$ [4] and $[(3,5\text{-}MC_2Ph)_2qpy^{2+}]Cl_2 \bullet 5CD_3OD$ [11]. Also, while these two previously reported structures show planar 2,2′-bpy units, the $(4\text{-}(CO_2H)Ph)_2qpyH^{3+}$ molecule displays a twist of ca. 19.5° about the central C–C bond. As for Ph_2qpy^{2+} and $(3,5\text{-}MC_2Ph)_2qpy^{2+}$, the rest of the molecule is strongly twisted, but asymmetrically so; the dihedral angles are 34.9° and 17.2° within the 4,4′-bpy fragments and 36.0° and 42.1° between the pyridyl and attached phenyl rings. All other geometric parameters for these three qpy-based dications are very similar.

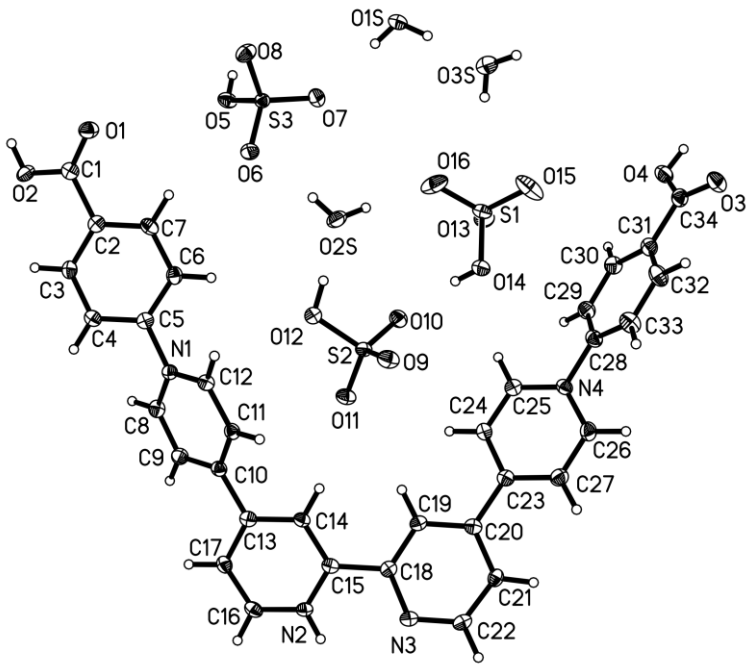

Fig. 7. Representation of the molecular structure of $[(4\text{-}(CO_2H)Ph)_2qpyH^{3+}][HSO_4]_3 \bullet 3H_2O$ (50% probability ellipsoids).

3.6. Theoretical Calculations

DFT and TD-DFT calculations were carried out by using Gaussian 03 [18] to probe the electronic structures and optical properties of the complexes in **7** and **14**. The results of these calculations are presented in Table 4.

On optimisation, the structures of the complexes in salts **7** and **14** (denoted **7′** and **14′**) adopt a pseudo-octahedral geometry where the N_{py}– Ru– N_{py} angle is less than 80° within the chelate and *ca*. 100° outside it. Both complexes show a similar extent of twisting between the rings of each quaterpyridinium ligand. The dihedral angles range from 29–33° within the 4,4′-bpy units, while larger angles are observed between the phenyl rings and the adjacent pyridyl rings; 47– 48° for **7′** and 51– 52° for **14′**.

Table 4

Data obtained from TD-DFT calculations on the complexes **7′** (MPW1PW91/Def2-SVP) and **14′** (MPW1PW91/DGDZVP) in DMSO (CPCM).[a]

complex	ΔE (eV)	λ (nm)	f_{os}	major contributions (%)	μ_{12} (D)
7′	1.53	810	0.14	HOMO → LUMO (29) HOMO → LUMO+1 (6) HOMO → LUMO+2 (5)	4.99
	1.54	805	0.04	HOMO → LUMO+1 (35)	2.56
	1.84	674	0.10	HOMO → LUMO+2 (11) HOMO–1 → LUMO+1 (10) HOMO–2 → LUMO (11)	3.77
	1.85	670	0.08	HOMO → LUMO+3 (31) HOMO–1 → LUMO (6)	3.47
	1.96	633	0.63	HOMO–2 → LUMO (24) HOMO–1 → LUMO+1 (13)	9.24
	2.13	582	0.16	HOMO–1 → LUMO (19) HOMO–1 → LUMO+2 (18)	4.39
	2.17	571	0.28	HOMO–1 → LUMO+1 (7) HOMO–1 → LUMO+3 (36)	5.86
	2.23	556	0.11	HOMO–2 → LUMO+3 (27) HOMO–2 → LUMO+2 (15)	3.67
	2.56	484	0.06	HOMO → LUMO+5 (45)	2.39
	3.58	346	0.40	HOMO–6 → LUMO+1 (7) HOMO–5 → LUMO+1 (16) HOMO–4 → LUMO (13)	5.45
	3.73	332	0.45	HOMO–8 → LUMO (5) HOMO–7 → LUMO (17) HOMO–5 → LUMO+3 (6)	5.63
	3.83	324	0.25	HOMO–8 → LUMO (10) HOMO–5 → LUMO+3 (7)	4.13
14′	1.70	729	0.13	HOMO → LUMO (43)	4.42
	1.74	713	0.04	HOMO → LUMO+1 (41)	2.47
	1.97	629	0.04	HOMO–2 → LUMO (12) HOMO–1 → LUMO+1 (32)	2.38
	2.00	620	0.17	HOMO–2 → LUMO (31) HOMO–1 → LUMO+1 (11)	4.67

	2.04	608	0.16	HOMO → LUMO+2 (36) HOMO → LUMO+3 (8)	4.58
	2.18	569	0.19	HOMO–2 → LUMO+1 (7) HOMO–1 → LUMO (12) HOMO → LUMO+3 (16)	4.75
	2.29	541	0.16	HOMO–2 → LUMO+2 (9) HOMO–1 → LUMO+2 (10) HOMO–1 → LUMO+3 (27)	4.34
	2.55	486	0.04	HOMO–3 → LUMO+1 (48)	1.97
	2.80	443	0.04	HOMO–3 → LUMO+3 (47)	1.84
	3.14	395	0.26	HOMO–5 → LUMO (25) HOMO–4 → LUMO+1 (17)	4.66
	3.28	378	0.25	HOMO–6 → LUMO (41)	4.49
	3.43	361	0.46	HOMO–5 → LUMO+2 (15) HOMO–4 → LUMO+3 (24)	5.95
	3.63	341	0.21	HOMO–8 → LUMO (5) HOMO–7 → LUMO+1 (6) HOMO–6 → LUMO+2 (7) HOMO → LUMO+8 (13) HOMO → LUMO+9 (6)	3.92
	3.67	338	0.23	HOMO–8 → LUMO (14) HOMO–7 → LUMO+1 (12) HOMO → LUMO+8 (6)	4.04

[a] f_{os} = oscillator strength; μ_{12} = transition dipole moment.

For both **7′** and **14′**, the inclusion of a DMSO solvent continuum (CPCM) in the TD-DFT calculations was necessary to obtain adequate correlations with the experimental UV–vis spectra (Figure 8). Such an effect has been noted previously for similar Ru complexes [33]. Without the CPCM, the transition energies are red-shifted by several hundreds of nanometres. The difference is more significant for **14′**, so the larger DGDZVP basis set was employed to give better results for this complex. This basis set has been used previously to good effect on the N3 dye by De Angelis and co-workers [34].

For the **7′**, the main calculated electronic transitions (500–700 nm) are not separated sufficiently to accurately replicate the shape of the experimental spectrum, although the energies correlate approximately with the observed bands (Fig. 8a). Two major transitions are calculated in this region with several flanking ones contributing to the overall broad shape. The low energy tail which extends up to 900 nm in the experimental spectrum is modelled with two transitions at around 800 nm, with one being dominant. A dense

collection of higher energy transitions forms the band below 400 nm. For **14′**, the low energy tail which extends up to 900 nm is well replicated by the TD calculation, although the shape of the profile at higher energy provides a less accurate fit. The low energy tail is again modelled by two transitions above 700 nm, which are significantly blue-shifted with respect to the equivalent ones in **7′** (see below). The main visible band is modelled by four dominant transitions between 500 and 650 nm, with several more transitions contributing to the overall shape. The high energy band below 400 nm comprises many transitions, although the energy of the predicted band is slightly red-shifted with respect to the experimental spectrum.

Figs. 9 and 10 depict the HOMOs and LUMOs of **7′** and **14′**, respectively. For **7′**, the lowest energy transitions have HOMO → LUMO, LUMO+1 and LUMO+2 character. The HOMO is made up of the Ru d_{xy} orbital in a π-antibonding arrangement with two Cl p orbitals. The LUMOs are π*-orbitals occupying one arm of each quaterpyridinium ligand, with only small contributions from the metal. For **14′**, the lowest energy transitions have HOMO → LUMO and LUMO+1 character, and the HOMO comprises the Ru d_{xy} orbital antibonding with the two NCS^- ligands. Within the NCS^- ligand, the C− N is π-bonding and the S p orbital is antibonding with respect to the C− N fragment. As for **7′**, the LUMOs of **14′** are π*-orbitals which are situated mainly on one arm of each ligand. In neither case are any components of the LUMOs based on the phenyl rings. As expected, the HOMO is stabilised in **14′** in comparison to **7′** by *ca*. 16 eV which is mirrored in the relative blue-shift of the low energy band in the UV–vis spectrum of **14′**. This result is consistent with the experimental spectra (see above).

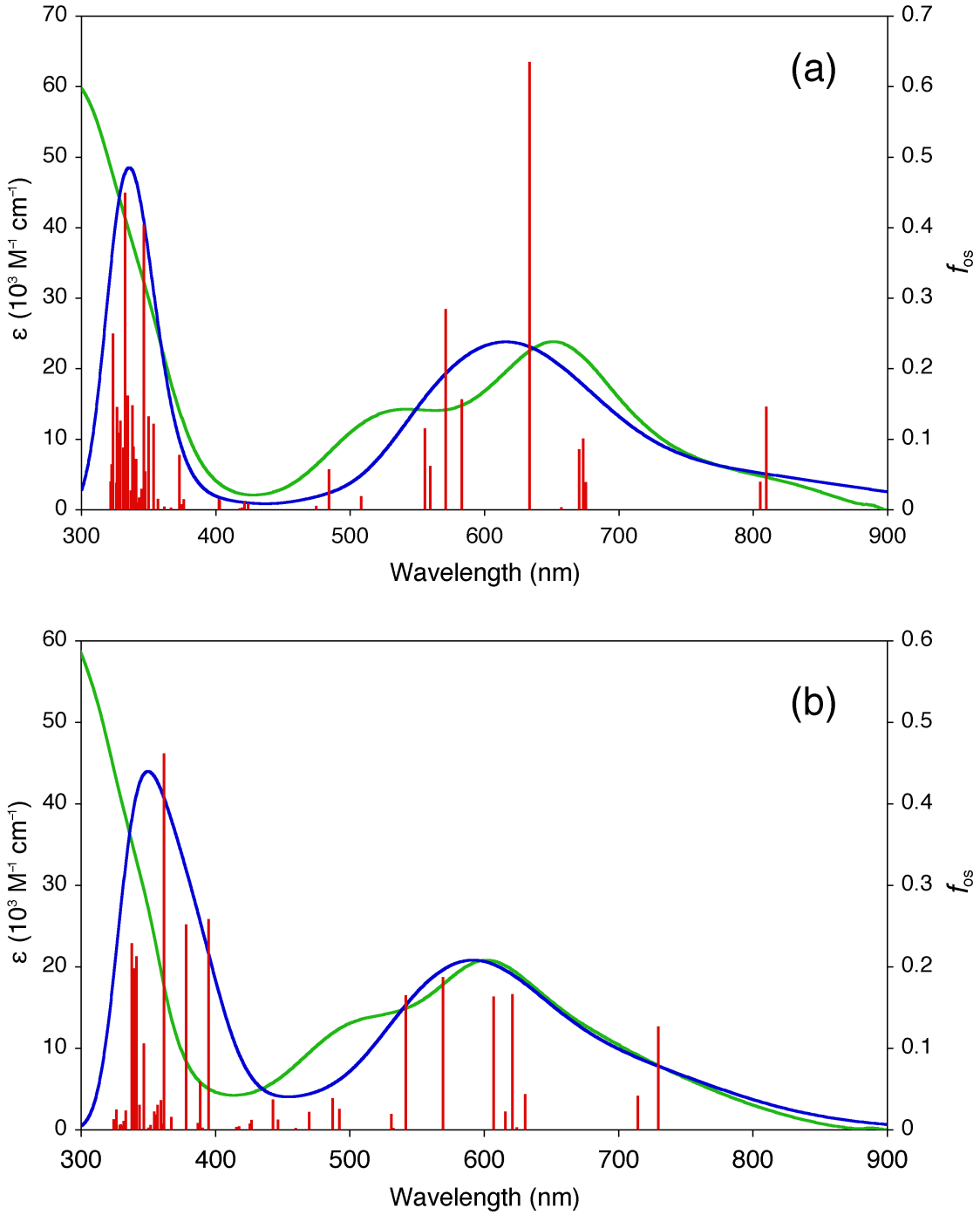

Fig. 8. TD-DFT-calculated (blue) and experimental (green) UV–vis spectra of (a) **7′** and (b) **14′** in DMSO. The ε-axes refer to the experimental data only and the vertical axes of the calculated data are scaled to match the main experimental absorptions. The f_{os} axes refer to the individual calculated transitions (red).

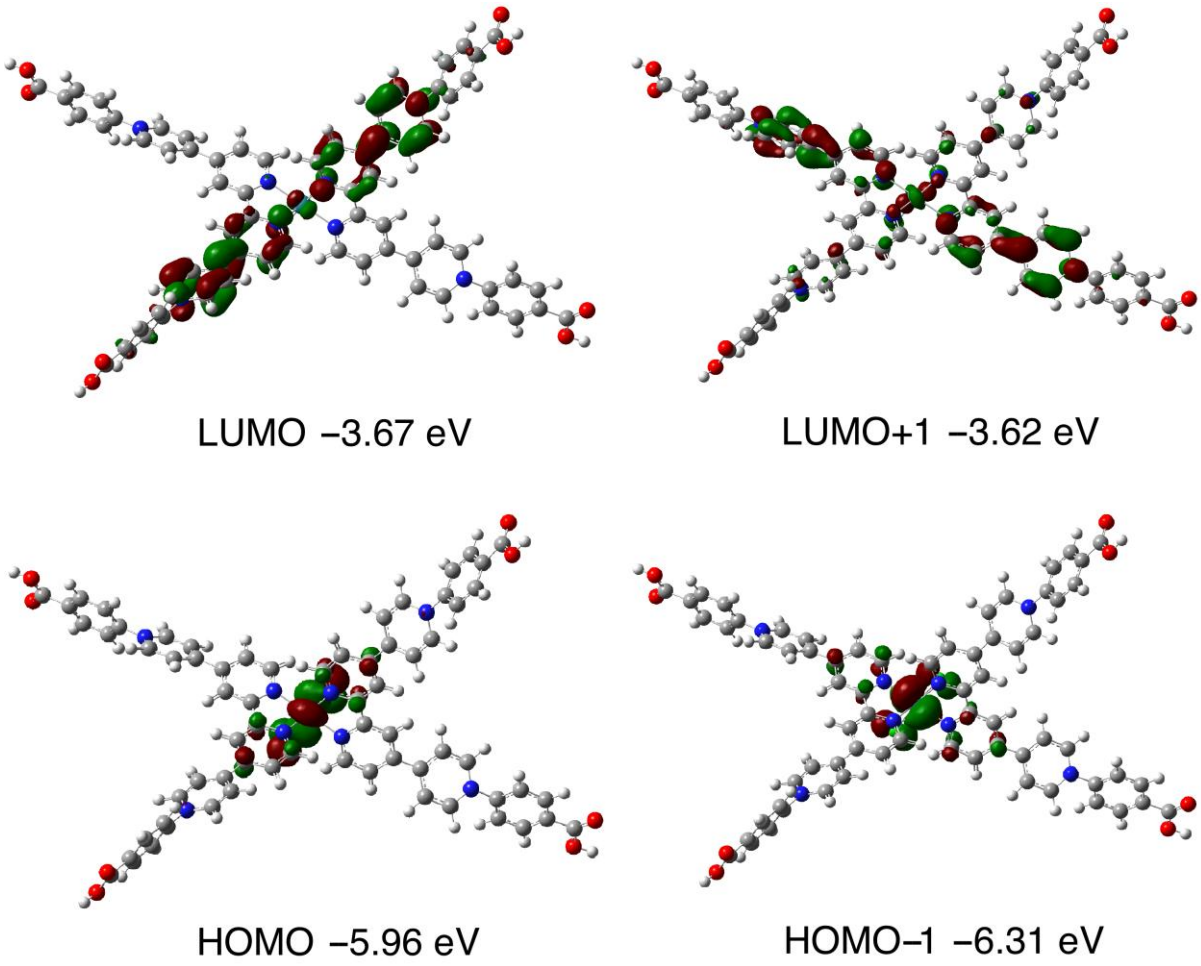

Fig. 9. Contour surface diagrams of some of the orbitals involved in the transitions of **7′** contributing to the low energy absorption above 450 nm (isosurface value 0.03 au).

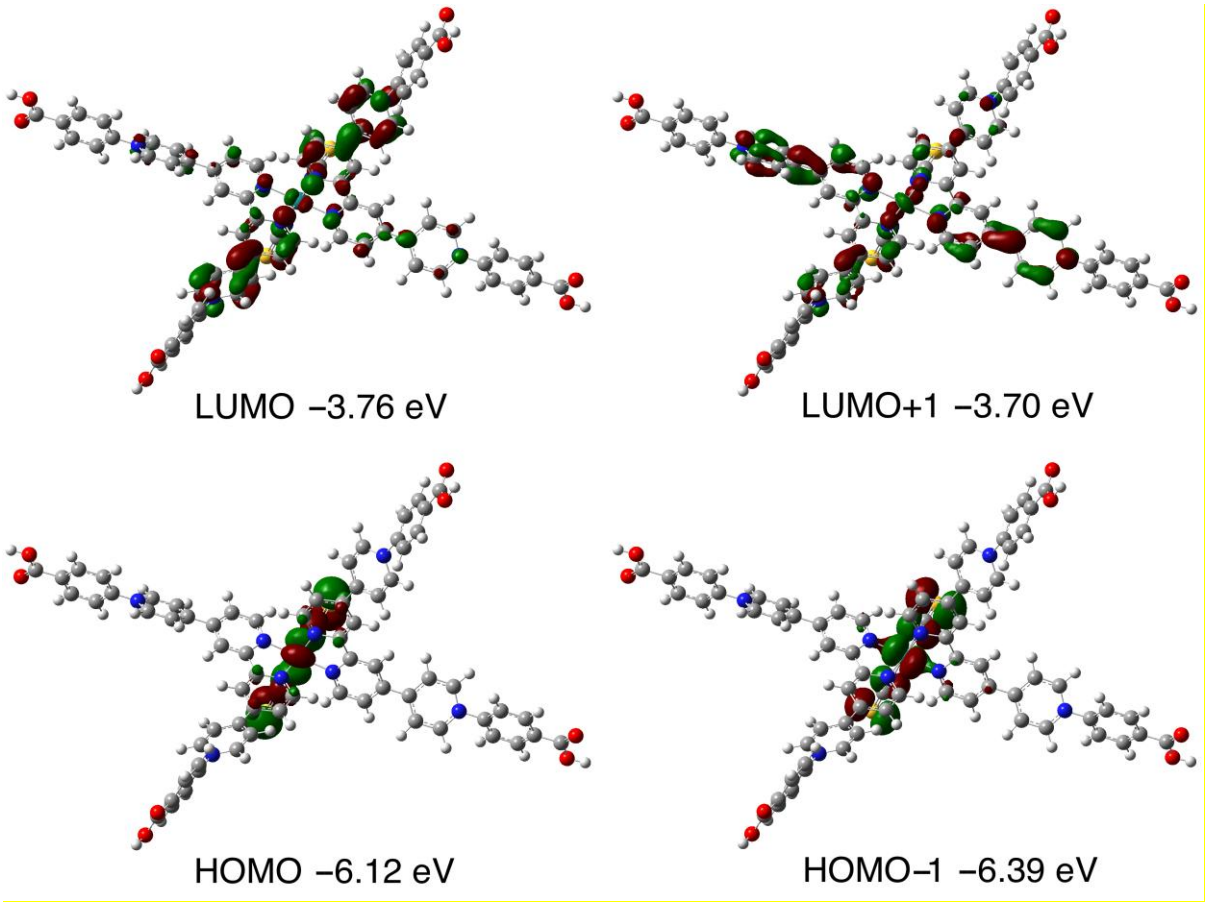

Fig. 10. Contour surface diagrams of some of the orbitals involved in the transitions of **14′** contributing to the low energy absorption above 450 nm (isosurface value 0.03 au).

3.7 Photosensitization Studies

The two carboxylic acid-functionalised compounds, **7** and **14**, were tested initially as sensitizers on TiO_2 electrodes. The current-voltage curves of the cells based on these dyes are shown in Fig. 11a, and the photovoltaic performance of the cells is summarised in Table 5.

The performance of the TiO_2-based cells fabricated with **7** and **14** is extremely poor when compared with the reference dye N719. As for the related *cis*-$[Ru^{II}(2,2'\text{-bpy})_2(R_2qpy^{2+})]^{4+}$ complexes in **19** and **20** [11], the IPCE could not be measured due to the exceptionally low photocurrents. It is worth mentioning that the composition of the

electrolyte used for testing **7** and **14** was specially designed to decrease the conduction band energy of TiO_2. The results obtained are very disappointing, since it was anticipated that the absorption behaviour of these dyes might lead to good photovoltaic performances. The likely explanation for these observations is inefficient electron injection into the TiO_2 surface, possibly due to poor matching between the excited state energy levels of the dyes and the conduction band of TiO_2. Also, the presence of long and twistable bridges between the Ru^{II} centre and the TiO_2 surface can be expected to hinder electronic coupling. Notably, the DFT-derived LUMOs include no electron density on the phenyl rings. Although the theoretical calculations do not predict the excited-state orbital energies or redox potentials of the dyes, they do help to explain qualitatively their very low photosensitizing efficiencies.

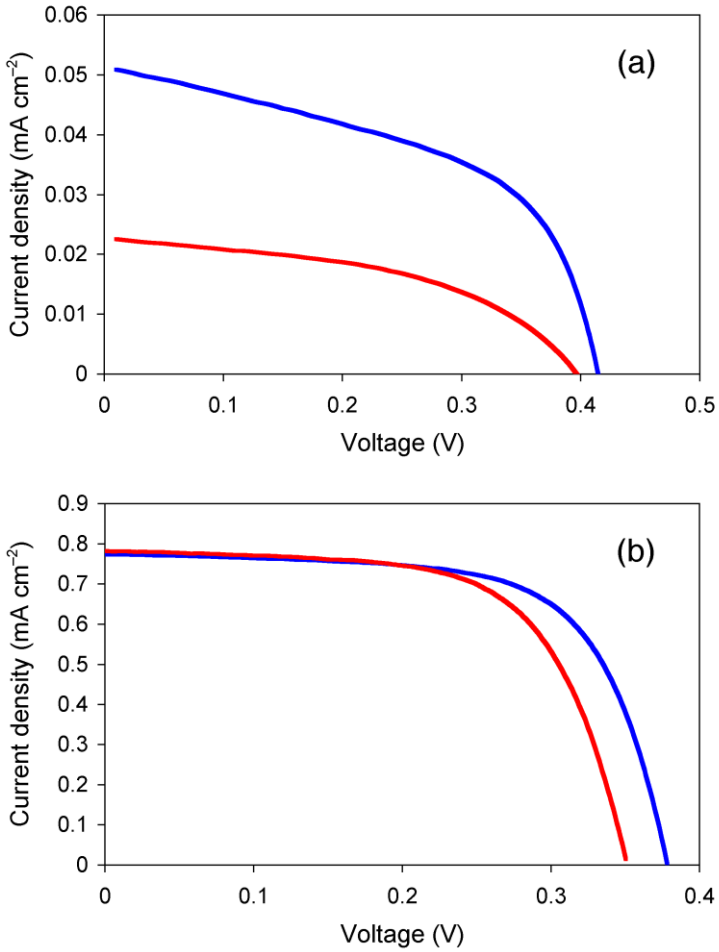

Fig. 11. Current-voltage curves of solar cells fabricated with **7** (blue) and **14** (red) under AM 1.5G illumination: (a) TiO_2-based; (b) ZnO-based.

Table 5

Photovoltaic performance parameters for solar cells fabricated with **7**, **14** and the reference dye N719, measured under AM 1.5G illumination (100 mW cm^{-2}).[a]

dye	J_{sc} (mA cm^{-2})	V_{oc} (mV)	FF (%)	η (%)
7[b]	0.050	410	24.4	0.005
14[b]	0.023	395	28.6	0.003
N719[b]	13.8	750	79.5	8.23
7[c,d]	0.774	378	66.7	0.2
14[c,d]	0.782	351	64.5	0.2
14[c,e]	0.960	297	58.4	0.2
14[c,f]	0.671	384	62.7	0.2
N719[c,d]	5.63	603	60.2	2.0

[a] J_{sc} = short-circuit current density; V_{oc} = open-circuit voltage; FF = fill factor; η = power conversion efficiency. N719 is the bis-[NBu^n_4] salt of the doubly deprotonated N3 dye.

[b] TiO_2-based cells.

[c] ZnO-based cells.

[d] With electrolyte 3.

[e] With electrolyte 1.

[f] With electrolyte 2.

Sensitization studies with **7** and **14** have been carried out also by using ZnO instead of TiO_2 electrodes. These two related semiconductor materials have significantly different characteristic parameters [35]. The dye immersion time for the ZnO-coated substrates was only 1 h (cf. 16 h for TiO_2-coated substrates), as the chemical stability of ZnO is rather poor when compared to TiO_2 [36]. The current-voltage curves of the cells are shown in Fig. 11b, and the photovoltaic performance is summarised in Table 5.

The photosensitizing performances of **7** and **14** are improved dramatically on ZnO when compared with TiO_2 electrodes (Table 5). This difference indicates that electron injection is more effective when the dyes are attached to ZnO surfaces. The overall efficiency of our new dyes is still an order of magnitude below that of N719, but the improvements observed are encouraging and indicate that changing other aspects of the cell could prove worthwhile. From the perspective of molecular design, significant scope exists to tune both the energy levels and the electron donor-acceptor coupling. For example, using

N-(2-carboxyvinyl)- instead of *N*-arylpyridinium groups can be expected to enhance the electronic coupling and therefore electron injection into the semiconductor. Also, replacing the carboxylic acid groups with phosphonic acid or catechol anchoring units may prove beneficial [37].

4. Conclusion

A series of complexes *cis*-$[Ru^{II}X_2(R_2qpy^{2+})_2]^{4+}$ (R_2qpy^{2+} = a 4,4′:2′,2″:4″,4‴-quaterpyridinium ligand, X = Cl^- or NCS^-) has been synthesised and characterised as their PF_6^- salts by using ^1H NMR spectroscopy and other techniques. The UV–vis spectra of these complex salts show an intense intraligand $\pi \rightarrow \pi^*$ absorption and low energy MLCT bands with two maxima. As X is kept constant within the two series, the MLCT bands red-shift as the electron-acceptor strength of the pyridinium units increases. Also, the MLCT energies are higher for the dithiocyanato species than for their dichloro analogues. The electronic absorption properties of the two carboxylic acid-functionalised compounds **7** and **14** are superior to that of the N3 dye, with broader and more intense profiles in the visible and NIR regions. Cyclic voltammetry reveals quasi-reversible or reversible $Ru^{III/II}$ oxidation waves, together with multiple, irreversible ligand-based reductions. Both of the trends shown by the MLCT energies are reflected in the measured reduction potentials. A single-crystal X-ray structure has been determined for the serendipitously produced compound $[(4\text{-}(CO_2H)Ph)_2qpyH^{3+}][HSO_4]_3 \bullet 3H_2O$, a protonated form of one of the proligand salts. TD-DFT calculations with a DMSO solvent continuum give adequate correlations with the experimental UV–vis spectra for the complexes in **7** and **14**. The complex salts **7** and **14** have been tested as photosensitizers on TiO_2- and ZnO-coated electrodes. Although the photovoltaic performance of these new sensitizers is disappointing, substantial improvements occur on moving from TiO_2 to ZnO. Inefficient electron injection is probably due to weak electronic coupling with the semiconductor surfaces, as indicated by the DFT-derived LUMOs that feature no electron density near the carboxylic acid anchoring groups. It is also possible that the energetic alignment of the excited-state donor orbitals with the conduction

band edges of the semiconductors may be non-ideal. Nevertheless, substantial scope exists for improving the sensitizing properties by judicious changes in the molecular structure, with the aim of maintaining and exploiting the highly attractive electronic absorption properties.

Acknowledgment

We thank the EPSRC for support in the form of a PhD studentship (YTT) and also DyStar UK Ltd and the University of Manchester for funding a PhD studentship (OAB). We are grateful to Dr Joseph J. W. McDouall (Manchester) for advice concerning TD-DFT calculations. The work in Bath was supported by the EPSRC (grant EP/E035469/1). EG and JAA thank the Ministerio de Ciencia e Innovación of Spain for project HOPE CSD2007-00007 (Consolider-Ingenio 2010), CTQ2009-10477 (TRANSLIGHT), and a FPU studentship, and Junta de Andalucia (Andalusian Regional Government) under projects P07-FQM-02595, P07-FQM-02600, and P09-FQM-04938.

Supplementary data

CCDC 892472 contains the supplementary crystallographic data for this paper. These data can be obtained free of charge via www.ccdc.cam.ac.uk/data_request/cif, data_request@ccdc.cam.ac.uk, or by contacting The Cambridge Crystallographic Data Centre, 12, Union Road, Cambridge CB2 1EZ, UK; fax: +44 1223 336033.

References

[1] (a) Md.K. Nazeeruddin, M. Grätzel, In Comprehensive Coordination Chemistry II, Vol. 9. J.A. McCleverty, T.J. Meyer, Eds., Pergamon Press, Oxford, UK, 2004, pp. 719–758;

(b) N. Robertson, Angew. Chem. Int. Ed. 45 (2006) 2338;

(c) J.R. Durrant, S.A. Haque, E. Palomares, Chem. Commun. (2006) 3279;

(d) L.M. Peter, J. Phys. Chem. C 111 (2007) 6601;

(e) Special issue on organic photovoltaics. Acc. Chem. Res. 42 (2009) 1689–1857;

(f) A. Hagfeldt; G. Boschloo; L.-C. Sun; L. Kloo; H. Pettersson, Chem. Rev. 110 (2010) 6595;

(g) R.R. Lunt, T.P. Osedach, P.R. Brown, J.A. Rowehl, V. Bulović, Adv. Mater. 23 (2011) 5712;

(h) J.N. Clifford, E. Martínez-Ferrero, A. Viterisi, E. Palomares, Chem. Soc. Rev. 40 (2011) 1635;

(i) A. Reynal, E. Palomares, Eur. J. Inorg. Chem. (2011) 4509;

(j) M.J. Griffith, K. Sunahara, P. Wagner, K. Wagner, G.G. Wallace, D.L. Officer, A. Furube, R. Katoh, S. Mori, A.J. Mozer, Chem. Commun. 48 (2012) 4145;

(k) Y.-S. Yen, H.-H. Chou, Y.-C. Chen, C.-Y. Hsu, J.T. Lin, J. Mater. Chem. 22 (2012) 8734;

(l) P.G. Bomben, K.C.D. Robson, B.D. Koivisto, C.P. Berlinguette, Coord. Chem. Rev. 256 (2012) 1438;

(m) P. Broadwith, Chemistry World, June 2012, pp 52–55.

[2] B. O'Regan, M. Grätzel, Nature 353 (1991) 737.

[3] (a) B.J. Coe, In Nonlinear Optical Properties of Matter: From Molecules to Condensed Phases; M.G. Papadopoulos, J. Leszczynski, A.J. Sadlej, Eds.; Springer: Dordrecht, 2006, pp. 571–608;

(b) B.J. Coe, Coord. Chem. Rev. 256 (2012) in press.

[4] B.J. Coe, J.A. Harris, L.A. Jones, B.S. Brunschwig, K. Song, K. Clays, J. Garín, J. Orduna, S.J. Coles, M.B. Hursthouse, J. Am. Chem. Soc. 127 (2005) 4845.

[5] B.J. Coe, J.A. Harris, B.S. Brunschwig, I. Asselberghs, K. Clays, J. Garín, J. Orduna, J. Am. Chem. Soc. 127 (2005) 13399.

[6] B.J. Coe, M. Samoc, A. Samoc, L.-Y. Zhu, Y.-P. Yi, Z.-G. Shuai, J. Phys. Chem. A 111 (2007) 472.

[7] Other recent examples:

(a) B.J. Coe, Acc. Chem. Res. 39 (2006) 383;

(b) H.S. Kim, K.W. Sohn, Y. Jeon, H. Min, D. Kim, K.B. Yoon, Adv. Mater. 19 (2007) 260;

(c) H. Figi, L. Mutter, C. Hunziker, M. Jazbinšek, P. Günter, B.J. Coe, J. Opt. Soc. Am. B 25 (2008) 1786;

(d) J.-D. Compain, P. Mialane, A. Dolbecq, J. Marrot, A. Proust, K. Nakatani, P. Yu, F. Sécheresse, Inorg. Chem. 48 (2009) 6222;

(e) B.J. Coe, J. Fielden, S.P. Foxon, B.S. Brunschwig, I. Asselberghs, K. Clays, A. Samoc, M. Samoc, J. Am. Chem. Soc. 132 (2010) 3496.

(f) B.J. Coe, J. Fielden, S.P. Foxon, J.A. Harris, M. Helliwell, B.S. Brunschwig, I. Asselberghs, K. Clays, J. Garín, J. Orduna, J. Am. Chem. Soc. 132 (2010) 10498.

(g) P.-J. Kim, J.-H. Jeong, M. Jazbinšek, S.-B. Choi, I.-H. Baek, J.-T. Kim, F. Rotermund, H. Yun, Y.S. Lee, P. nter, O.-P. Kwon, Adv. Funct. Mater. 22 (2012) 200;

(h) K. De Mey, J. Perez-Moreno, J.E. Reeve, I. Lopez-Duarte, I. Boczarow, H.L. Anderson, K. Clays, J. Phys. Chem. C 116 (2012) 13781.

[8] Selected examples:

(a) Y.-H. Kim, A. Das, H.-Y. Zhang, P.K. Dutta, J. Phys. Chem. B 109 (2005) 6929;

(b) P.P. Lainé, F. Bedioui, F. Loiseau, C. Chiorboli, S. Campagna, J. Am. Chem. Soc. 128 (2006) 7510;

(c) J.M. Weber, M.T. Rawls, V.J. MacKenzie, B.R. Limoges, C.M. Elliott, J. Am. Chem. Soc. 129 (2007) 313;

(d) H.-Y. Zhang, C.S. Rajesh, P.K. Dutta, J. Phys. Chem. C 113 (2009) 4623;

(e) J.D. Henrich, H.-Y. Zhang, P.K. Dutta, B. Kohler, J. Phys. Chem. B 114 (2010) 14679;

(f) J. Fortage, C. Peltier, F. Nastasi, F. Puntoriero, F. Tuyèras, S, Griveau, F. Bedioui, C. Adamo, I. Ciofini, S. Campagna, P.P. Lainé, J. Am. Chem. Soc. 132 (2010) 16700.

[9] O.A. Blackburn, B.J. Coe, V. Hahn, M. Helliwell, J. Raftery, Y.T. Ta, L.M. Peter, H.-X. Wang, J.A. Anta, E. Guillén, Dyes Pigments 92 (2011) 766.

[10] N. Baumann, P.S. Gamage, T.N. Samarakoon, J. Hodgson, J. Janek, S.H. Bossmann, J. Phys. Chem. C 114 (2010) 22763.

[11] B.J. Coe, E.C. Harper, M. Helliwell, Y.T. Ta, Polyhedron 30 (2011) 1830.

[12] I.P. Evans, A. Spencer, G. Wilkinson, J. Chem. Soc., Dalton Trans. (1973) 204.

[13] SAINT (Version 6.45), Bruker AXS Inc.; Madison: Wisconsin, USA, 2003.

[14] SADABS (Version 2.10), Bruker AXS Inc.; Madison: Wisconsin, USA, 2003.

[15] G.M. Sheldrick, Acta Crystallogr. Sect. A 46 (1990) 467.

[16] G.M. Sheldrick, SHELXS 97, Programs for Crystal Structure Analysis (Release 97-2); University of Göttingen: Göttingen, Germany, 1997.

[17] SHELXTL (Version 6.10), Bruker AXS Inc.; Madison: Wisconsin, USA, 2000.

[18] Gaussian 03, Revision C.02, M.J. Frisch, G.W. Trucks, H.B. Schlegel, G.E. Scuseria, M.A. Robb, V.G. Cheeseman, J.A. Montgomery, T. Vreven Jr., K.N. Kudin, J.C. Burant, J.M. Millam, S.S. Iyengar, J. Tomasi, V. Barone, B. Mennucci, M. Cossi, G. Scalmani, N. Rega, G.A. Petersson, H. Nakatsuji, M. Hada, M. Ehara, K. Toyota, R. Fukuda, J. Hasegawa, M. Ishida, T. Nakajima, Y. Honda, O. Kitao, H. Nakai, M. Klene, X. Li, J.E. Knox, H.P. Hratchian, J.B. Cross, C. Adamo, J. Jaramillo, R. Gomperts, R.E. Stratmann, O. Yazyev, A.J. Austin, R. Cammi, C. Pomelli, J.W. Ochterski, P.Y. Ayala, K. Morokuma, G.A. Voth, P. Salvador, J.J. Dannenberg, V.G. Zakrzewski, S. Dapprich, A.D. Daniels, M.C. Strain, O. Farkas, D.K. Malick, A.D. Rabuck, K. Raghavachari, J.B. Foresman, J.V. Ortiz, Q. Cui, A.G. Baboul, S. Clifford, J. Cioslowski, B.B. Stefanov, G. Liu, A. Liashenko, P. Piskorz, I. Komaromi, R.L. Martin, D.J. Fox, T. Keith, M.A. Al-Laham, C.Y. Peng, A. Nanayakkara, M. Challacombe, P.M.W. Gill, B. Johnson, W. Chen, M.W. Wong, C. Gonzalez, J.A. Pople; Gaussian, Inc., Wallingford CT, 2004.

[19] A.D. Becke, Phys. Rev. A 38 (1988) 3098.

[20] J.P. Perdew, Phys. Rev. B 33 (1986) 8822.

[21] F. Weigend, R. Ahlrichs, Phys. Chem. Chem. Phys. 7 (2005) 3297.

[22] V. Barone, M. Cossi, J. Phys. Chem. A 102 (1998) 1995.

[23] M. Cossi, N. Rega, G. Scalmani, V. Barone, J. Comput. Chem. 24 (2003) 669.

[24] C. Adamo, V. Barone, J. Chem. Phys. 108 (1998) 664.

[25] N. Godbout, D.R. Salahub, J. Andzelm, E. Wimmer, Can. J. Chem. 70 (1992) 560.

[26] N.M. O'Boyle, A.L. Tenderholt, K.M. Langner, J. Comput. Chem. 29 (2008) 839.

[27] See for example: A. Kukrek, D. Wang, Y.-J. Hou, R.-F. Zong, R. Thummel, Inorg. Chem. 45 (2006) 10131.

[28] (a) S.K.S. Yadav, U.C. Agarwala, Polyhedron 3 (1984) 1;
(b) M. Kakoti, S. Chaudhury, A.K. Deb, S. Goswami, Polyhedron 12 (1993) 783;
(c) O. Kohle, S. Ruile, M. Grätzel, Inorg. Chem. 35 (1996) 4779;
(d) Md.K. Nazeeruddin, M. Grätzel, J. Photochem. Photobiol. A: Chem. 145 (2001) 79;
(e) L. Vandenburgh, M.R. Buck, D.A. Freedman, Inorg. Chem. 47 (2008) 9134;
(f) T.P. Brewster, W.-D. Ding, N.D. Schley, N. Hazari, V.S. Batista, R.H. Crabtree, Inorg. Chem. 50 (2011) 11938.

[29] M.K. Nazeeruddin, A. Kay, I. Rodicio, R. Humphry-Baker, E. Müller, P. Liska, N. Vlachopoulos, M. Grätzel, J. Am. Chem. Soc. 115 (1993) 6382.

[30] V. Shklover, M.-K. Nazeeruddin, S.M. Zakeeruddin, C. Barbé, A. Kay, T. Haibach, W. Steurer, R. Hermann, H.-U. Nissen, M. Grätzel, Chem. Mater. 9 (1997) 430.

[31] G. Wolfbauer, A.M. Bond, D.R. MacFarlane, Inorg. Chem. 38 (1999) 3836.

[32] Selected examples:
(a) B.N. Figgis, B.W. Skelton, A.H. White, Aust. J. Chem. 31 (1978) 57;
(b) A.D. Burrows, R.W. Harrington, M.F. Mahon, Acta Crystallogr., Sect. C 55 (1999) 1921;
(c) I.A. Charushnikova, C. Den Auwer, Acta Crystallogr., Sect. E 60 (2004) m1775;
(d) L.-F. Ma, B.-T. Zhao, L.-Y. Wang, Anal. Sci. 21 (2005) x85;
(e) T. Kawasaki, T. Nishimura, T. Kitazawa, Bull. Chem. Soc. Jpn. 83 (2010) 1528.

[33] See for example: S. Fantacci, F. De Angelis, A. Selloni, J. Am. Chem. Soc. 125 (2003) 4381.

[34] F. De Angelis, S. Fantacci, A. Selloni, Chem. Phys. Lett. 389 (2004) 204.

[35] E. Guillén, L.M. Peter, J.A. Anta, J. Phys. Chem. C 115 (2011) 22622.

[36] K. Keis, J. Lindgren, S.-E. Lindquist, A. Hagfeldt, Langmuir 16 (2000) 4688.

[37] F. Ambrosio, N. Martsinovich, A. Troisi, J. Phys. Chem. Lett. 3 (2012) 1531.

Graphical Abstract

New complex salts *cis*-$[Ru^{II}X_2(R_2qpy^{2+})_2]^{4+}$ (R_2qpy^{2+} = a 4,4′:2′,2″:4″,4‴-quaterpyridinium ligand, X = Cl^- or NCS^-) have been prepared and studied by using techniques including UV–vis spectroscopy, cyclic voltammetry and TD-DFT calculations. Photosensitizing behaviour of two carboxylic acid-functionalised derivatives has been assessed on both TiO_2 and ZnO.

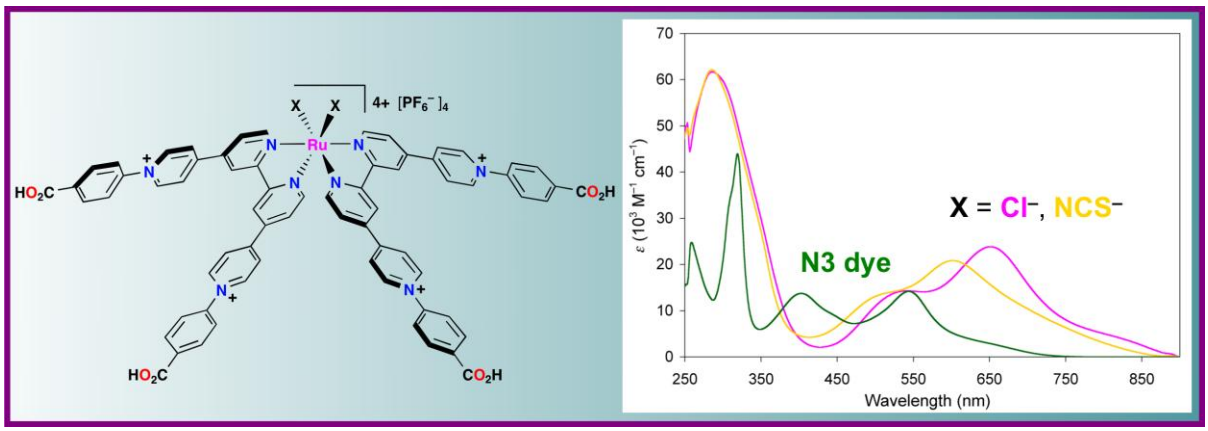

CIF File (Required if manuscript contains crystal structure(s))

Click here to download CIF File (Required if manuscript contains crystal structure(s)): Blackburn-Polyhedron.cif

CIF Validation Report (Recommended if manuscript contains crystal structure(s))

Click here to download CIF Validation Report (Recommended if manuscript contains crystal structure(s)): Blackburn-Polyhedron